

# 1 Organic matter quality of deep permafrost carbon - a study 2 from Arctic Siberia

3  
4 J. Strauss<sup>1\*</sup>, L. Schirrmeister<sup>1</sup>, K. Mangelsdorf<sup>2</sup>, L. Eichhorn<sup>3</sup>, S. Wetterich<sup>1</sup> and  
5 U. Herzschuh<sup>1</sup>

6 [1]{Alfred Wegener Institute Helmholtz Centre for Polar and Marine Research, Periglacial  
7 Research Unit Potsdam, Telegrafenberg A 43, Potsdam, Germany}

8 [2]{Helmholtz Centre Potsdam GFZ German Research Centre for Geosciences,  
9 Telegrafenberg, 14473 Potsdam, Germany}

10 [3]{International Max Planck Research School for Global Biogeochemical Cycles (Max-  
11 Planck-Institute for Biogeochemistry and Friedrich Schiller University), Burgweg 11, 07749,  
12 Jena, Germany}

13 Correspondence to: J. Strauss (Jens.Strauss@awi.de)

## 14 15 **Abstract**

16 The organic carbon (OC) pool accumulated in Arctic permafrost (perennially frozen ground)  
17 equals the carbon stored in the modern atmosphere. To give an idea of how Yedoma region  
18 permafrost could respond under future climatic warming, we conducted a study to quantify  
19 the organic matter quality (here defined as the intrinsic potential to be further transformed,  
20 decomposed, and mineralized) of late Pleistocene (Yedoma) and Holocene (thermokarst)  
21 deposits on the Buor Khaya Peninsula, northeast Siberia. The objective of this study was to  
22 develop a stratigraphic classified organic matter quality characterization. For this purpose the  
23 degree of organic matter decomposition was estimated by using a multiproxy approach. We  
24 applied sedimentological (grain-size analyses, bulk density, ice content) and geochemical  
25 parameters (total OC, stable carbon isotopes ( $\delta^{13}\text{C}$ ), total organic carbon : nitrogen (C/N)  
26 ratios) as well as lipid biomarkers (*n*-alkanes, *n*-fatty acids, hopanes, triterpenoids, and  
27 biomarker proxies/indices: average chain length, carbon preference index (CPI), and higher  
28 plant fatty acid index (HPFA)). Our results show that the Yedoma and thermokarst organic  
29 matter qualities for further decomposition exhibit no obvious degradation - depth trend.

1 Relatively, the C/N, and  $\delta^{13}\text{C}$ , values and the HPFA index show a significantly better  
2 preservation of the organic matter stored in thermokarst deposits compared to Yedoma  
3 deposits. The CPI data suggest less degradation of the organic matter from both deposits with  
4 a higher value for Yedoma organic matter. As the interquartile ranges of the proxies mostly  
5 overlap, we interpret this as to indicate comparable quality for further decomposition for both  
6 kinds of deposits with likely better thermokarst organic matter quality. Supported by principal  
7 component analyses, the sediment parameters and quality proxies of Yedoma and thermokarst  
8 deposits could not be separated without ambiguity from each other. This revealed that the  
9 organic matter vulnerability is heterogeneous and depends on different decomposition  
10 trajectories and the previous decomposition and preservation history. Elucidating this was one  
11 of the major novelties of our multiproxy study. With the addition of biomarker data, it was  
12 possible to show that permafrost organic matter degradation likely occurs via a combination  
13 of (uncompleted) degradation cycles or a cascade of degradation steps rather than as a linear  
14 function of age or sediment facies. We conclude that the amount of organic matter in the  
15 studied sediments is high for mineral soils and of good quality and therefore susceptible to  
16 future decomposition. The missing depth trends reveal that permafrost acts like a giant  
17 freezer, preserving the constant quality of ancient organic matter. When undecomposed  
18 Yedoma organic matter is mobilized via thermokarst processes, the fate of this carbon  
19 depends largely on the environmental conditions; the carbon could be preserved in an  
20 undecomposed state till refreezing occurs. If modern input has occurred, thermokarst organic  
21 matter could be of a better quality for future microbial decomposition than that found in  
22 Yedoma deposits.

23

## 24 **1 Introduction**

25 During the late Quaternary, the rate of organic matter decomposition in the Arctic has been  
26 slower than plant growth, sedimentation, and freezing rates. Thus, a large pool of organic  
27 carbon (OC) accumulated in the Arctic and was deeply sequestered in the permafrost.  
28 Hugelius et al. (2014) estimates an OC storage of 1300 Gt for the circum-Arctic permafrost  
29 region with ~850 Gt OC sequestered in permafrost. This is approximately the carbon stored in  
30 the modern atmosphere (Dlugokencky and Tans, 2014). During warming and permafrost  
31 thawing, this formerly cryo-sequestered OC gradually entered the modern biogeochemical  
32 cycle by microbial turnover. By thawing and microbial activity, the permafrost deposits can

1 turn from a carbon sink to a source (Schuur et al., 2009), releasing greenhouse gases such as  
2 carbon dioxide and methane to the atmosphere. Besides the near-surface carbon pool  
3 representing the uppermost 3 m below surface, and because of rapid permafrost thaw like  
4 thermokarst and thermoerosion, deep OC pools, especially those held in ice-rich permafrost  
5 deposits in the Yedoma region, are of great significance for current concerns about the effects  
6 of global warming. According to Strauss et al. (2013) and Hugelius et al. (2013), the Yedoma  
7 region is defined as the area of potential distribution of late Pleistocene ice-rich and organic-  
8 rich silty deposits (Yedoma) covering large areas in Siberia and Alaska. Estimates of OC  
9 stored in the Yedoma region amount to  $83\pm 12$  Gt for late Pleistocene Yedoma deposits (ages  
10 shown in Table 1). Due to Holocene warming, subsequent ground ice melt and surface  
11 subsidence, thermokarst basins formed and were partly occupied by lakes. Holocene  
12 thermokarst deposits (ages shown in Table 1) contain  $130\pm 29$  Gt organic carbon. In total, the  
13 Yedoma region extends to an area of about 1,387,000 km<sup>2</sup> of which about 70 % is already  
14 affected by permafrost degradation (thermokarst) (Strauss et al., 2013). Kuhry et al. (2009)  
15 and Schirrmeister et al. (2011a) showed that Yedoma deposits accumulated at fast rates,  
16 implying a short time for the organic matter to decay before it became locked into a  
17 perennially-frozen state. Therefore, the organic matter availability for microorganisms is  
18 expected to be excellent, resulting in great vulnerability to warming ground conditions (Mu et  
19 al., 2014). To elucidate how Yedoma region permafrost could respond under conditions of  
20 future climatic warming, we studied the organic matter degradation state of Yedoma and its  
21 Holocene degradation features (called thermokarst deposits) on Buor Khaya Peninsula,  
22 Eastern Laptev Sea. As mentioned above, Strauss et al. (2013) found that thermokarst  
23 deposits contain the quantitatively more important carbon pool, but the unsolved question is  
24 this: Is the thermokarst organic matter pool as degradable as the frozen late Pleistocene  
25 Yedoma, or has the most labile carbon already been emitted due to thermokarst degradation  
26 processes? In both kinds of deposits the OC was deeply (deeper than 3 m) incorporated into  
27 permafrost (Schirrmeister et al., 2013; Strauss et al., 2013). As shown by models and  
28 extrapolation from recent observations, the more southern portions of Yedoma deposits  
29 thawed during the last deglaciation, resulting in large emissions of greenhouse gases to the  
30 atmosphere (Walter et al., 2007a; Ciais et al., 2012; Walter Anthony et al., 2014). Recent  
31 ground warming has been observed in the permafrost zone (Romanovsky et al., 2010), and  
32 incubation experiments reveal that permafrost warming is accompanied by a substantial  
33 outgassing of greenhouse gases (Lee et al., 2012; Knoblauch et al., 2013; Schädel et al.,

1 2014). As an illustration of the important influence of ground temperature on organic matter  
2 degradation, a higher respiration rate at greater depth close to the permafrost table  
3 (Mangelsdorf et al., 2009; Waldrop et al., 2010) was found inside the seasonally-thawed  
4 active layer and interpreted as a greater lability of the organic matter close to the perennially  
5 frozen ground. Focusing on permafrost deposits in the Laptev Sea region, which includes our  
6 Buor Khaya study site, Schirrmeister et al. (2011a) characterize the Yedoma region  
7 permafrost organic matter as weakly decomposed.

8 Biomarkers are used for paleoenvironmental reconstruction of terrestrial permafrost  
9 (Andersson et al., 2011) or characterization of permafrost organic matter degradation  
10 (Andersson and Meyers, 2012; Vonk et al., 2013; Routh et al., 2014). In our study we  
11 estimate molecular markers (*n*-alkanes, *n*-fatty acids, hopanes, and triterpenoids) and use  
12 biomarker proxies/indices (absolute lipid concentration, average chain length (ACL), carbon  
13 preference index (CPI), hop-17(21)-ene, higher plant fatty acid (HPFA) index, and an  
14 Oleanen ratio) to test whether they are useful mirrors of organic matter decomposition, i.e.  
15 organic matter state of degradation in permafrost deposits. Rather established methods, both  
16 cryolithological (grain-size analyses, bulk density, ice content) and biogeochemical (total  
17 organic carbon (TOC<sub>wt%</sub>), stable carbon isotope ratios ( $\delta^{13}\text{C}$  in TOC), total nitrogen (TN), and  
18 TOC<sub>wt%</sub>/TN (C/N) ratios), are applied to our sample set. Finally, principal components  
19 analysis (PCA) highlights the relationships between different organic matter degradation  
20 proxies.

21 Because the future feedback from the Yedoma region permafrost OC to climate forcing is  
22 driven by both (1) the pool size, estimated to be ~211 Gt (Strauss et al., 2013), and (2) the  
23 state of degradation of OC stored in the studied deposits, the objective of this study is the  
24 development of a stratigraphically differentiated organic matter quality characterization using  
25 sample material representative of widespread Yedoma and thermokarst permafrost. We  
26 hypothesize increased organic matter degradation during thermokarst processes, but also  
27 increased organic matter input during climatically favorable Holocene times.

## 28 **2 Material and methods**

### 29 **2.1 Study area**

30 The Buor Khaya Peninsula study site (71°34'N, 132°12'E) is located in the northeastern part  
31 of Siberia (Fig. 1). Buor Khaya Peninsula is framed by the Laptev Sea, a shallow

1 epicontinental part of the Arctic Ocean, and geologically by two rift structures (Drachev et al.,  
2 1998). Buor Khaya is underlain by continuous permafrost with ground temperatures of less  
3 than -11°C (Drozhdov et al., 2005). The permafrost thicknesses is estimated to be between 450  
4 and 650 m (Romanovskii et al., 2004). Stratigraphically, outcrops from two sediment units are  
5 distinguished and studied; (1) ice-rich permafrost, called Yedoma deposits, and (2) deposits in  
6 permafrost rapid thaw features, generalized as thermokarst deposits. Three profiles of  
7 thermokarst deposits (in a thermokarst basin: Buo-01 and Buo-05; initial thermokarst on top  
8 of a Yedoma hill: Buo-03) and two profiles of Yedoma deposits (Buo-02, Buo-04) were  
9 studied and sampled. Fig. 1 shows an overview of the sampled profiles and their position  
10 relative to each other.

## 11 **2.2 Field work**

12 Field studies were undertaken in summer 2010 at outcrops situated at the western coast of the  
13 Buor Khaya Peninsula. The sediment of the profiles and sub-profiles, exposed at the cliff wall  
14 or partly in thermokarst mounds in thaw slumps, were dug by spades and cleaned with hacks.  
15 The cryolithology, sediment characteristics, and visible organic matter in the sediments of the  
16 chosen sequences were surveyed and described. Moreover, the profiles were photographed  
17 and sketched. Sub-profiles were stacked together to create composite profiles. Sampling  
18 positions in neighboring sub-profiles were correlated by height estimation using measuring  
19 tape. The upper edge of each profile was calibrated with tacheometer measurements (Günther  
20 et al., 2012). In the field laboratory all sample volumes were measured with a balance and  
21 Archimedes principle, and the absolute ice content was determined by drying the sample. In  
22 total, 91 samples were taken and kept cool for transport to laboratories for further analysis.  
23 Detailed sampling positions for each profile are shown in Strauss and Schirrmeister (2011).

## 24 **2.3 Indicators of organic matter quality for further decomposition**

25 To validate and to extend the sedimentological approach used, and to estimate the organic  
26 matter quality for further decomposition, lipid biomarkers were measured to estimate the  
27 degree of organic matter degradation. For biomarker studies we used a “fingerprint” approach  
28 by focusing on identifiable markers related to the state of organic matter degradation. Below,  
29 the utilized geochemical indicators and biomarkers are described.

### 1 **2.3.1 Grain-size analyses**

2 Grain sizes were analyzed using a laser particle sizer (LS 200, Beckmann-Coulter) between  
3 0.375 and 1000  $\mu\text{m}$  (Fig. 2, S1). Grain-size calculations were done after Folk and Ward  
4 (1957) using Gradistat v8 (Blott and Pye, 2001). A detailed description of these analytical  
5 techniques is given in the supplement (supplement section 1.1).

### 6 **2.3.2 Elemental composition**

7 To determine the total elemental carbon and total nitrogen (TN) content, the samples were  
8 measured by a carbon-nitrogen-sulphur analyzer (Vario EL III, Elementar).  $\text{TOC}_{\text{wt}\%}$  was  
9 measured with a TOC analyzer (Vario Max C, Elementar). The volumetric TOC content  
10 ( $\text{TOC}_{\text{kg}/\text{m}^3}$ ) was calculated according to Strauss et al. (2013). A detailed description of this  
11 techniques is given in the supplement (supplement section 1.2).

12 The TOC/TN (C/N) ratio has been used as a general indicator of the degree of organic matter  
13 decomposition (Stevenson, 1994). Based on the assumption that organic matter components  
14 are degraded selectively, degradation modifies elemental compositions and hence C/N in  
15 deposits. Because a decrease in the C/N ratio has been observed in aerated deposits with  
16 microbial immobilization of TN (nitrogen stays in the system) accompanied by the re-  
17 mineralization of TOC (Sollins et al., 1984) and  $\text{CO}_2$  emission, this ratio is used in the  
18 following way: The higher the C/N ratio, the lower the degree of decomposition.

### 19 **2.3.3 Bulk density and volumetric carbon content**

20 BD was calculated using equation 1.

$$21 \text{BD} [10^3\text{kg}/\text{m}^3] = \frac{\text{sample dry weight} [10^3\text{kg}]}{\text{sample volume} [\text{m}^3]} \quad (1)$$

22 Estimating the BD is required to convert the measured-weight-based  $\text{TOC}_{\text{wt}\%}$  content per  
23 sample to a volume-based value. Thus, the  $\text{TOC}_{\text{kg}/\text{m}^3}$  was calculated according to equation 2:

$$24 \text{TOC}_{\text{kg}/\text{m}^3} = \text{BD} [10^3\text{kg}/\text{m}^3] \times \frac{\text{TOC}_{\text{wt}\%}}{100} \quad (2)$$

### 25 **2.3.4 Carbon isotope studies**

26 Stable TOC carbon isotopes were determined with a Finnigan MAT Delta-S mass  
27 spectrometer combined with a FLASH elemental analyzer and a CONFLO III gas mixing

1 system. A detailed method is given in the supplement (supplement section 1.4). The stable  
2 carbon isotopes of OC reflect (1) initial contribution from different plant species and plant  
3 components, and (2) subsequent degradation processes (Gundelwein et al., 2007). Assuming  
4 constant photosynthetic isotope fractionation in source plants in the region ( $C_3$  plants are  
5 ubiquitous in the Arctic, Tieszen (1973)), we use  $\delta^{13}C$  ratios as a degradation proxy. After  
6 Heyer et al. (1976), decomposition discriminates against the lighter isotope ( $^{12}C$ ), resulting in  
7 more negative  $\delta^{13}C$  ratios. Thus, this proxy is used in the following way: Lower (more  
8 negative)  $\delta^{13}C$  values are connected to less degraded material, while higher (less negative)  
9  $\delta^{13}C$  values reflect greater decomposition.

10 Ages were determined by radiocarbon dating of selected macroscopic plant remains  
11 performed at the Poznań Radiocarbon Laboratory, Poland (Goslar et al., 2004). The presented  
12 radiocarbon ages are uncalibrated ages; Table 1 includes calibrated ages as well. Radiocarbon  
13 ages are given in year before present (a BP).

### 14 **2.3.5 Lipid biomarkers**

15 To look more closely at the molecular composition, we used specific lipid biomarkers.  
16 Molecular fossils or biomarkers were studied by chromatography methods coupled with mass  
17 spectrometers. Characteristic fractions like *n*-alkanes, *n*-fatty acids, sterols, and hopanes were  
18 isolated. Because the  $TOC_{wt\%}$  in the profiles is not equally distributed, we calculated and  
19 visualized the biomarker concentration as  $\mu g/gTOC_{wt\%}$  and  $\mu g/gSediment$  ( $\mu g/gSed$ ). For the  
20 results, we focus on  $\mu g/gTOC_{wt\%}$ . Every radiocarbon-dated sample and additional samples  
21 were used for biomarker analysis. In total 25 biomarker samples were analyzed. Independent  
22 from  $TOC_{wt\%}$ , the sample selection for biomarkers was based on stratigraphic position with  
23 the aim to cover the maximum time period.

### 24 **Extraction and fraction separation**

25 For lipid biomarker analyses 2-12 g of ground sediment was weighed in an extraction cell  
26 with an accelerated solvent extractor (ASE 200, Dionex). Samples were extracted with  
27 dichloromethane/methanol (99:1). Each sample was held in a static phase for 20 minutes at 75  
28 °C (after 5 minutes heating, no preheating) at a pressure of 5 MPa. Afterwards, the dissolved  
29 compounds were concentrated with a Turbo Vap (Zymark) closed cell concentrator and  
30 further dried by evaporating the solvent in a stream of nitrogen gas. After that, internal  
31 standards (5 $\alpha$ -androstane for the aliphatic fraction, ethylpyrene for the aromatic fraction, 5 $\alpha$ -

1 androstan-17-on for nitrogen-, sulfur-, and oxygen- (NSO-) containing compounds, and erucic  
2 acid for the NSO fatty acid fraction) were added. The amount of internal standards depended  
3 on the TOC<sub>wt%</sub> content (<10wt%: 8µg; >10 to ≤25wt%: 20µg; >25wt%: 50µg). After the  
4 removal of the *n*-hexane-insoluble fraction (by the addition of a large excess of *n*-hexane,  
5 called ‘asphaltene’ precipitation), the hexane-soluble portion of the extract was separated by  
6 medium-pressure liquid chromatography (MPLC; (Radke et al., 1980) into fractions of  
7 different polarity (aliphatic and aromatic hydrocarbons as well as polar hetero (NSO)  
8 components). Afterwards, the NSO fraction was split into a fatty acids and an alcohol fraction  
9 using a KOH-impregnated silica gel column (Schulte et al., 2000).

10 For this study, the focus was placed on the aliphatic fraction (containing *n*-alkanes and  
11 triterpenoid compounds) and the NSO fraction (containing *n*-fatty acids). The fractions were  
12 measured by gas chromatography–mass spectrometry (GC–MS). All compounds of interest  
13 were identified using the Xcalibur software (Thermo Fisher Scientific).

#### 14 **GC-MS measurement and compound quantification**

15 The *n*-alkanes, *n*-alcohols, hopenes (hop-17(21)-ene), and other triterpenoids (β-amyrin  
16 (olean-12-en-3β-ol), Olean-12-ene, and Olean-13(18)-ene) were measured with a GC-MS  
17 system (GC: Trace GC Ultra; MS: DSQ, both Thermo Fisher Scientific). Prior to the  
18 measurements, the *n*-fatty acids were methylated with diazomethane and the alcohols were  
19 silylated with *N*-methyl-*N*-trimethylsilyltrifluoroacetamide (MSTFA). The GC was equipped  
20 with a programmable temperature vaporization (PTV) injector system (starting temperature of  
21 50 °C; heating rate of 10°C/sec to 300°C; isothermal holding time of 10 minutes; operated in  
22 splitless mode) and a fused silica capillary column (SGE BPX5, 50 m length, 0.22 mm inner  
23 diameter, 0.25 µm film thickness). For the measurements the GC oven was programmed with  
24 a starting temperature of 50°C, a heating rate of 3°C/min to 310°C, and an isothermal holding  
25 time of 30 minutes. Helium with a constant flow rate of 1 ml/min was used as a carrier gas.  
26 For the *n*-fatty acid fraction a different temperature program (starting temperature of 50°C, 1  
27 min isotherm, heating rate of 3°C/min to 350°C, isothermal holding time 25 minutes) was  
28 used. For compound identification, the gas chromatograph was linked to a mass spectrometer,  
29 which was operated in electron impact ionization mode at 70 eV. The temperature of the ion  
30 source was set to 230°C. Full scan mass spectra were recorded from *m/z* 50 to 600 Da at a  
31 scan rate of 2.5 scans/sec. For the *n*-fatty acids fraction the scan rate was *m/z* 50 to 650 Da.



1 Quantification of *n*-alkanes, *n*-fatty acids, and  $\beta$ -amyryn was done in the GC-MS total ion  
2 current chromatogram by relating the peak area of the target compound to the peak area of an  
3 internal standard of known concentration. Other triterpenoids like Olean-12-ene, Olean-  
4 13(18)-ene, and hopene were quantified using the *m/z* 191 mass trace relative to the peak area  
5 of the  $\beta,\beta$ -diploptene (in the *m/z* 191 mass trace), the concentration of which was calculated  
6 in the total ion current chromatogram relative to the internal standard (5 $\alpha$ -androstane).

## 7 **2.3.6 Biomarker proxies/indices**

### 8 **Absolute lipid concentration**

9 The absolute lipid concentration is used as rough estimator of organic matter quality for  
10 degradation in the following sense: The higher the concentration, the better the conservation  
11 of the lipid, and the better the quality of the organic matter.

### 12 **Carbon preference index**

13 The CPI was introduced by Bray and Evans (1961) as the ratio of odd- to neighboring even-  
14 numbered alkanes, which is a measure of the alteration of organic matter. Here we use the  
15 improved formula after Marzi et al. (1993). In addition, we also applied the CPI for fatty acids  
16 in which even-numbered fatty acids predominate over adjacent odd *n*-fatty acids (Glombitza  
17 et al., 2009).

$$18 \text{ CPI} = \frac{(\sum_{i=n}^m C_{2i+1}) + (\sum_{i=n+1}^{m+1} C_{2i+1})}{2 \times (\sum_{i=n+1}^{m+1} C_{2i})} \quad (3)$$

19 *n*: starting dominating chain length/2; *m*: ending dominating chain length/2; *i*:  
20 index (carbon number); *C*: concentration

21 The CPI is used as a degradation/alteration proxy by quantifying the odd/even (*n*-alkanes, Fig.  
22 S2) or even/odd (*n*-fatty acids, Fig. S3) of the carbon chains (Bray and Evans, 1961;  
23 Glombitza et al., 2009). A low CPI means mature/degraded organic matter (e.g. CPI of crude  
24 oil ~1).

### 25 **Average chain length**

26 As introduced by Poynter (1989), the *n*-alkane ACL value is the concentration-weighted mean  
27 of different carbon chain lengths in a geological sample. For *n*-alkanes we use the C<sub>23</sub>-C<sub>33</sub>  
28 interval, for *n*-fatty acids the C<sub>20</sub>-C<sub>34</sub>:

$$1 \quad ACL = \frac{\sum i \times C_i}{\sum C_i} \quad (4)$$

2 *i*: index (carbon number); *C*: concentration

3 The ACL is a rough OC source parameter. A schematic showing different chain lengths in  
4 different organisms is given in Fig. S4. The higher C<sub>3</sub> land plants are expected to have an  
5 ACL of ~28-29.

### 6 **Hop-17(21)-ene**

7 We use hop-17(21)-ene as another marker for low-maturity organic material. The hop-17(21)-  
8 ene is produced by bacteria. The assumption here is that during degradation and diagenesis  
9 the hop-17(21)-ene will be transformed into saturated hopane (Luo et al., 2012).

### 10 **Higher Plant Fatty Acid index**

11 The ratio of the major even wax alcohols over the sum of major odd wax alkanes plus even  
12 alcohols was introduced by Poynter (1989) as the Higher Plant Alcohol (HPA) index. It is  
13 applied as an indicator for chemical degradation of the wax components. Based on this index,  
14 but using fatty acids instead of alcohols, we developed the HPFA index. The general  
15 assumption for this index is that it reflects the preservation degree of the organic matter due to  
16 the higher lability of *n*-fatty acids in relation to *n*-alkanes.

$$17 \quad HPFA = \frac{\sum \text{n-fatty acids}_{C_{24}, C_{26}, C_{28}}}{\sum \text{n-fatty acids}_{C_{24}, C_{26}, C_{28}} + \sum \text{n-alkanes}_{C_{27}, C_{29}, C_{31}}} \quad (5)$$

18 The HPFA ratio cannot be considered an absolute index of degradation, but is an indicator of  
19 the relative amounts of the more labile fatty acids that remain in a sample. Since *n*-alkanes are  
20 preserved preferentially compared to *n*-fatty acids, a decrease in this index indicates increased  
21 decomposition (the more degraded, the lower the HPFA index).

### 22 **Oleanen ratio**

23 β-amyrin (olean-12-en-3β-ol) is a triterpenoid produced by higher land plants. As a first  
24 degradation step, β-amyrin is expected to lose its hydroxy-group and will be transformed to  
25 Olean-12-ene. A second step would be a shift of the double bond forming Olean-13(18)-ene.  
26 Thus, fresh organic material is associated with a lower oleanen ratio, while more degraded  
27 organic matter is reflected in a higher ratio. This index is calculated:

$$28 \quad \text{oleanen ratio [\%]} = \frac{\text{Olean-12-ene} + \text{Olean-13(18)-ene}}{\beta\text{-amyrin}} \times 100 \quad (6)$$

## 1 **Acetate**

2 Pore water was obtained from each sample by centrifugation in specific pore water tubes.  
3 Water extracts were analyzed twice using ion chromatography with conductivity detection  
4 (ICS 3000, Dionex). An analytical column (AS 11 HC, 2 × 250 mm, Dionex) was used at  
5 constant 35°C. The sample was eluted with KOH solution of varying concentration over time.  
6 The initial concentration was 1.4 mM. Between 0 and 6 minutes, the KOH solution was  
7 increased at a constant rate to 1.6 mM. Between 6 and 12 minutes the solution was increased  
8 to 10.0 mM KOH and a concentration of 15.0 mM KOH was reached at 22 minutes. After 32  
9 minutes, 60.0 mM KOH concentration was achieved, and maintained for 1 minute, followed  
10 by a rapid decrease to 1.4 mM after 33 minutes where samples were fixed for 45 minutes to  
11 equilibrate the system. For quantification of acetate, standards containing the investigated  
12 compound were measured. The standard deviation of the sample and of standard  
13 quantification was <5%. Because acetate can act as excellent feedstock for microbes (Smith  
14 and Mah, 1980; Vieth et al., 2008) and it has been shown that acetate was rapidly consumed  
15 in the presence of oxygen and nitrate (Kuesel and Drake, 1995), we use the acetate pore water  
16 concentrations in the different deposits as a parameter to assess the quality of the organic  
17 matter and to compare the potential of the different deposits for future microbial degradation.

## 18 **2.4 Statistical methods**

### 19 **2.4.1 Significance testing**

20 For testing the samples concerning their statistical distribution, the Shapiro-Wilk normality  
21 test was applied. Because of non-normal distribution, we used the Mann-Whitney-Wilcoxon  
22 test for significance testing of Yedoma and thermokarst samples. For comparing the different  
23 five profiles, we used Kruskal-Wallis rank sum test.

### 24 **2.4.2 Principal component analysis**

25 Multivariate statistical techniques, like the PCA used here, allow the analysis of multiple  
26 variables in order to investigate connections between the different degradation proxies. Prior  
27 to the PCA, concentration data were transformed using a log (x+1) transformation. As the  
28 square root transformation is commonly applied to count data, especially if the values are  
29 mostly rather small, we decided to use this weaker (compared to logarithm) transformation for  
30 the TOC (wt% and kg/m<sup>3</sup>) data. Both transformations were applied to reduce right skewness and

1 to put the parameters on the same scale. We performed three PCA runs. First, a PCA of the  
2 sediment parameters was implemented to infer differences between Yedoma and thermokarst  
3 deposits. Second, a PCA of biomarker proxies was performed. For this purpose, other  
4 characteristics were added as supplementary variables ( $\text{TOC}_{\text{wt}\%}$ ,  $\text{TOC}_{\text{kg/m}^3}$ , C/N,  $\delta^{13}\text{C}$ , grain  
5 size, BD, ice content, and depth) without inclusion in the PCA calculation. These  
6 supplementary variables have no influence on the PCA and were plotted afterwards in the  
7 PCA biplot. Third, a PCA was conducted on samples of the major odd *n*-alkanes to infer  
8 possible changes of the source organisms with the same supplementary variables as described  
9 above to relate the different biomarker proxies to each other. Computations were performed  
10 using the “vegan” package of R software (Oksanen, 2013).

### 11 **3 Results**

12 Stratigraphically, there are two types of deposition units at the study site. The first unit is  
13 composed of Yedoma deposits. The second unit represents thermokarst deposits resulting  
14 from thermal degradation of Yedoma. Grain-size distributions (Fig. 2, S1) and PCA of  
15 sediments illustrate that thermokarst deposits are made up of degraded Yedoma sediments.  
16 After Gubin and Veremeeva (2010) and Zanina et al. (2011) the Yedoma deposits soil types  
17 are mainly less-developed cryopedoliths containing more-developed paleocryosol parts (Fig.  
18 3 and 4, labeled and grey-shaded areas).

#### 19 **3.1 Organic matter quality of Yedoma deposits**

##### 20 **3.1.1 Sedimentological and biogeochemical proxies**

21 The radiocarbon ages (Table 1, Fig. S5) of the Yedoma deposits range from infinite ages  
22 ( $>55,000$  a BP) at the very bottom to 30,100 a BP at the uppermost sampled Yedoma unit.  
23 This is comparable to other Yedoma sequences in the region (Schirrmeister et al., 2011b). The  
24 mean grain sizes show a decreasing trend in the Buo-04 lower Yedoma profile, from 28  $\mu\text{m}$  at  
25 the bottom to 11  $\mu\text{m}$  in the upper part of Buo-04-A. The Buo-02 Yedoma profile shows no  
26 trend, but exhibits a more heterogeneous mean-grain size including three maxima at 22.5 m  
27 above sea level (a.s.l.) (32  $\mu\text{m}$ ), 23.7 m a.s.l. (34  $\mu\text{m}$ ), and 25.5 m a.s.l. (33  $\mu\text{m}$ ).  
28 Nevertheless, all Yedoma deposit samples are classified as poorly-sorted medium-to-coarse  
29 silts with a stable low clay fraction ( $<15\%$ ).

1 The  $\text{TOC}_{\text{wt}\%}$  contents vary from 0.2 wt% at 5 m a.s.l to 24.0 wt% in a peaty paleocrysol  
2 horizon at 24 m a.s.l. (Fig. 3). The mean  $\text{TOC}_{\text{wt}\%}$  content is 2.4 wt% (median 0.97 wt%).  
3 Calculating the  $\text{TOC}_{\text{kg}/\text{m}^3}$  according to Strauss et al. (2013) by utilizing the BD (between 0.1  
4 and  $1.5 \cdot 10^3 \text{kg}/\text{m}^3$  ( $10^3 \text{kg}/\text{m}^3 = \text{g}/\text{cm}^3$ )) and ice content (without ice wedges; 21 to 90 vol%), the  
5 Yedoma sediments contain from 3 to 46 kg C/ $\text{m}^3$  with a mean of 14 kg C/ $\text{m}^3$  (median 9 kg  
6 C/ $\text{m}^3$ ). The maxima correspond to the peaty horizons with large  $\text{TOC}_{\text{wt}\%}$  contents and a low  
7 BD. Within the paleocrysol horizons, located at 6.8, 24.0 to 24.5, 24.8, and 27.8 to 28.9 m  
8 a.s.l., maxima in the C/N ratio are observable. The C/N range in these horizons is 8 to 31. In  
9 the cryopedolith profile parts the C/N maximum is reached at the lowermost Buo-04-C sub-  
10 profile (17.7 and 16.7). The C/N of the rest of the Yedoma profile falls between 4.1 (at Buo-  
11 02-C, 23.7 m a.s.l.) and 14.3 (below the paleocrysol at 23.5 m a.s.l.)

12 The  $\delta^{13}\text{C}$  of the Yedoma deposits ranges between -29.0 and -24.7 ‰. The minima fit well to  
13 the maxima of the C/N ratio in the paleocrysol horizons at 6.8, 24.0 to 24.5, 24.8, and 27.8 to  
14 28.9 m a.s.l. The minimum C/N of the Buo-02-C sub-profile corresponds approximately to  
15 the  $\delta^{13}\text{C}$  maximum (-25.0 to -24.7 ‰).

### 16 **3.1.2 Biomarker proxies/indices**

17 A series of long-chain *n*-alkanes that exhibit a strong odd-carbon preference ranging from *n*-  
18  $\text{C}_{21}$  to *n*- $\text{C}_{33}$  are recognized in all Yedoma samples (Fig. S2). Moreover, the *n*-alkanes show a  
19 unimodal distribution maximizing at the  $\text{C}_{27}$ ,  $\text{C}_{29}$ , or  $\text{C}_{31}$  *n*-alkane (Fig. S2). The *n*-fatty acids  
20 show strong even-over-odd carbon number predominance and a bimodal distribution ranging  
21 from  $\text{C}_{14}$  to  $\text{C}_{30}$  (Fig. S3). The maxima are generally located at *n*- $\text{C}_{16}$  in the lower carbon  
22 number range and at *n*- $\text{C}_{24}$  in the higher carbon number range. Total *n*-alkanes and *n*-fatty  
23 acids concentrations related to  $\text{TOC}_{\text{wt}\%}$  and sediment weight show a homogeneous pattern  
24 similar to that of the  $\text{TOC}_{\text{wt}\%}$  and C/N values. The *n*-alkane concentration ranges from 3 to 75  
25  $\mu\text{g}/\text{gSed}$  (mean 20  $\mu\text{g}/\text{gSed}$ ) and from 387 to 1715  $\mu\text{g}/\text{TOC}_{\text{wt}\%}$  (mean 1132  $\mu\text{g}/\text{TOC}_{\text{wt}\%}$ ). The  
26 *n*-fatty acids range from 4 to 306  $\mu\text{g}/\text{gSed}$  (mean 51  $\mu\text{g}/\text{gSed}$ ) and from 475 to 4669  $\mu\text{g}/\text{TOC}$   
27 (mean 2196  $\mu\text{g}/\text{TOC}_{\text{wt}\%}$ ).

28 This Yedoma series shows distinct preference between even and odd carbon. The mean CPI  
29 values of the *n*-alkanes (12.2, ranging between 8.3 and 15.9) are higher than the CPI values of  
30 the *n*-fatty acids (4.9, ranging between 3.8 and 7.6). Because *n*-fatty acids are functional  
31 compounds (including a functional group, e.g. a carboxyl group), their degradation rates are

1 much higher compared to those of *n*-alkanes (Poynter and Eglinton, 1990). This statement is  
2 also based on the assumption of similar sources. The ACL of the *n*-alkanes and *n*-fatty acids  
3 is very stable at around 28.4 (range 27.6 to 29.2) and 25.0 (range 23.8 to 25.6), respectively.  
4 Relatively higher hop-17(21)-ene concentrations are used as an indicator for lower organic  
5 matter degradation state. In the lower Yedoma profile the hop-17(21)-ene ranges from 0.0  
6  $\mu\text{g/gTOC}$  at the lowermost and uppermost samples (4.3 and 18.5 m a.s.l.) to the overall  
7 maximum at the Buor Khaya site (19.4  $\mu\text{g/gTOC}$ ) at 9.1 m a.s.l. At Buo-02, the hop-17(21)-  
8 ene concentration is lower compared to the other Yedoma profile with a mean of 1.9  
9  $\mu\text{g/gTOC}_{\text{wt}\%}$  and a maximum of 7.7  $\mu\text{g/gTOC}_{\text{wt}\%}$  in the potentially Holocene-contaminated  
10 uppermost sample. The HPFA ratio for the Yedoma samples is very stable around the mean  
11 value of 0.50 (median 0.54) with a minimum at 18.5 m a.s.l. (0.15) and a maximum at the  
12 uppermost sample (0.69) at 29.7 m a.s.l. For Yedoma, the Oleanen ratio is 0.0 (except a ratio  
13 of 10.0 at the uppermost sample). The acetate content of the Yedoma sample is between 0.6  
14 and 57.5 mg/L with a mean of 6.7 mg/L (median 1.2 mg/L).

## 15 **3.2 Organic matter quality of thermokarst deposits**

### 16 **3.2.1 Sedimentological and biogeochemical proxies**

17 The radiocarbon dating shows Holocene ages between  $8140\pm 50$  and  $3665\pm 35$  a BP (Fig. S6,  
18 Table 1). The lowermost Buo-05-C profile shows an age inversion for the two samples, (0.3  
19 and 2.2 m a.s.l.). The mean grain size at Buo-05 from the bottom to 6.7 m a.s.l. is 13  $\mu\text{m}$ .  
20 Above, the mean grain size increases to 19  $\mu\text{m}$ . The Buo-05 clay fraction is stable at a low  
21 level (<15%). The Buo-01 profile shows a very scattered grain size ranging from 4 to 44  $\mu\text{m}$   
22 mean grain size. For the whole dataset, there is a maximum in the clay fraction (35%) in the  
23 peat horizon at 8.7 m a.s.l. Buo-03 shows a slight decrease from 18 to 11  $\mu\text{m}$ . All thermokarst  
24 deposits are classified as (very) poorly-sorted silts. Similar to the Yedoma deposits, the BD of  
25 the thermokarst deposits is between 0.1 and 1.5  $10^3\text{kg/m}^3$  and the ice content (without the ice  
26 wedges) is 23 to 87 wt% (Fig. 4).

27 The mean  $\text{TOC}_{\text{wt}\%}$  contents of the thermokarst deposits, 4.7 wt% (median 1.7 wt%), are  
28 higher compared to Yedoma deposits, varying between 0.2 wt% and 43.0 wt%. Minimum and  
29 maximum  $\text{TOC}_{\text{wt}\%}$  both occur at Buo-01 and exhibit the same scatter as in the grain sizes.  
30  $\text{TOC}_{\text{kg/m}^3}$  ranges between 2.8 and 93.5  $\text{kg C/m}^3$  (mean 24  $\text{kg C/m}^3$ , median 19  $\text{kg C/m}^3$ ).

1 At Buo-05 the C/N ratio is stable around 9 to 10 (Fig. 4), except for a paleocryosol horizon at  
2 9.2 m a.s.l. that shows a value of 22. At Buo-01, the C/N ratio below the paleocryosol horizon  
3 is remarkably low, between 2 and 9, followed by the overall maximum in the peaty horizon  
4 with a ratio of 34. The Buo-03 cryopedolith samples show C/N ratios around 10, while the  
5 paleocryosol samples exhibit C/N ratios from 16 to 19. The  $\delta^{13}\text{C}$  values range between -29.5  
6 and -25.0 ‰, with minima corresponding to the C/N maxima at the paleocryosol horizons  
7 (anti-correlated to the C/N, Fig. 5a).

### 8 **3.2.2 Biomarker proxies/indices**

9 The absolute lipid concentration of *n*-alkanes are in the same range but slightly higher  
10 compared to the Yedoma profiles. The *n*-alkane average is 1275.7  $\mu\text{g/gTOC}_{\text{wt}\%}$  (median  
11 1260.1  $\mu\text{g/gTOC}_{\text{wt}\%}$ ), ranging from 599.7 (8.7 m a.s.l.) to 1907.2  $\mu\text{g/gTOC}_{\text{wt}\%}$  (29.5 m a.s.l.).  
12 The *n*-fatty acids average is nearly double that found in the Yedoma samples. On average,  
13 4096.1  $\mu\text{g/gTOC}_{\text{wt}\%}$  (median 3805.7  $\mu\text{g/gTOC}_{\text{wt}\%}$ ) are stored in the thermokarst deposits of  
14 Buor Khaya, ranging from 554.5 (uppermost Buo-01 sample) to 11013.3 (uppermost Buo-03  
15 sample)  $\mu\text{g/gTOC}_{\text{wt}\%}$ .

16 A series of long-chain *n*-alkanes were recognized in all thermokarst samples with a strong odd  
17 carbon number preference ranging from *n*-C<sub>21</sub> to *n*-C<sub>33</sub>. Nearly all samples show a unimodal  
18 distribution of *n*-alkanes maximized at C<sub>27</sub>, C<sub>29</sub>, or C<sub>31</sub> (Fig. S2). Sample Buo-03-A-03 alone  
19 does not fit into this scheme because it maximizes at *n*-C<sub>25</sub>. Compared to Yedoma samples,  
20 the short-chain fraction < *n*-C<sub>27</sub> is more pronounced (Fig. S2). The *n*-fatty acids show strong  
21 even-carbon-number preference and a bimodal distribution between *n*-C<sub>14</sub> and *n*-C<sub>30</sub> (Fig. S3),  
22 but the *n*-C<sub>16</sub> is less pronounced than in the Yedoma deposits. An exception to this is found in  
23 sample Buo-01-A-02, where the C<sub>16</sub> monomer reaches the overall maximum of the  
24 distribution. Apart from that, the maxima are generally located at the C<sub>24</sub> *n*-fatty acid.

25 The *n*-alkane CPI of thermokarst averages 9.6 (median 9.3) and is lower compared to the  
26 Yedoma deposits, although the CPI values are in the same range (between 7.0 and 15.3). The  
27 CPI of the fatty acids ranges from 4.0 to 9.0 (mean 5.3, median 4.9). The ACL of *n*-alkanes  
28 and fatty acids reveal a homogeneous signal between 27.2 and 29.2 (mean 28.3) for *n*-alkanes  
29 and 23.6 to 25.6 (mean 24.8) for *n*-fatty acids.

30 Except for the maximum value of 16.1  $\mu\text{g/gTOC}_{\text{wt}\%}$  at 8.7 m a.s.l., the hop-17(21)-ene  
31 concentration at Buo-05 varies between 0.1 and 4.9  $\mu\text{g/gTOC}_{\text{wt}\%}$ . Buo-01 paleocryosol values

1 are 0.9 (8.7 m a.s.l.) and 8.4 at the lowermost sample (7.8 m a.s.l.). For Buo-03 the hop-  
2 17(21)-ene concentration ranges from 5  $\mu\text{g/gTOC}_{\text{wt}\%}$  up to 8  $\mu\text{g/gTOC}_{\text{wt}\%}$ .

3 The HPFA ratio for the Buo-05 thermokarst samples is high, between 0.6 and 0.8; only the  
4 uppermost sample (9.3 m a.s.l.) shows a lower value of 0.2. The Buo-01 profile decreases  
5 from 0.7 at the lowest sample to 0.2 at the top. Buo-03 shows high parameter values of 0.8  
6 and 0.9. The Oleanen ratio for the thermokarst deposits ranges between 0 (Buo-01) and 13.8  
7 (Buo-03). The overall mean Oleanen ratio in thermokarst is 3.7 (median 2.2), which is  
8 remarkably higher compared to the Yedoma deposits.

9 The acetate content of the thermokarst samples is between 0.4 and 109.4 mg/L with a mean of  
10 23.5 mg/L (median 2.8 mg/L). Large acetate contents are found especially in the middle part  
11 of Buo-05, from 3.4 m a.s.l. (74.1 mg/L) to 6.1 m a.s.l. (109.4 mg/L), and in the uppermost  
12 Buo-03 sample (35.3 mg/L).

### 13 **3.3 Statistical methods**

#### 14 **3.3.1 Significance testing**

15 Except for the Yedoma CPI, the Yedoma HPFA and the thermokarst hop-17(21)-ene Shapiro-  
16 Wilk normality test reveals a non-normal distribution. Based on this, we chose non-parametric  
17 significance testing. This reveals significant differences for TOC, C/N,  $\delta^{13}\text{C}$  and HPFA on the  
18 stratigraphical level (Yedoma vs. thermokarst, Mann-Whitney-Wilcoxon test, Tab. S1). On  
19 the profile level, we found significant differences for C/N,  $\delta^{13}\text{C}$  and HPFA by applying the  
20 Kruskal-Wallis test (Tab. S1).

#### 21 **3.3.2 Principal component analyses**

22 The first PCA diagram (Fig. 6a) shows that thermokarst sediments, especially at Buo-05,  
23 could not be separated from Yedoma deposits. This diagram, including the first two principal  
24 components, explains 79 % (pc1 57%, pc2 22%) of the total data set variance. The second  
25 PCA diagram (Fig. 6b) illustrates that biomarker quality estimators in Yedoma samples have  
26 slightly lower variability because they cluster in an area at pc1 and pc2>0, while the  
27 thermokarst samples do not cluster. In this diagram 53 % of the data set variance is explained.  
28 Moreover, this PCA shows that there is good consistency between the  $\text{CPI}_{\text{alkane}}$  quality  
29 estimator and the C/N ratio (Fig. 6b). The PCA of the *n*-alkane chain length (Fig. 6c) shows  
30 that the best separating variables for thermokarst are the shorter-chain *n*-alkanes ( $\text{C}_{17}$ ,  $\text{C}_{19}$ , and



1 C<sub>21</sub>), contrary to C<sub>29</sub> for the majority of the Yedoma samples. The pc1 explains 39% and pc2  
2 explains 29% (total 68%) of the data set variance.

3

## 4 **4 Discussion**

5 The Buor Khaya Peninsula is a typical Yedoma hill - thermokarst basin landscape of the  
6 Yedoma region (Strauss et al., 2013). The Yedoma deposits cover ~15% of the peninsula  
7 (Günther et al., 2013), which is less than the Yedoma region mean of 30%, but inside the  
8 overall range of Yedoma deposit coverage (Grosse et al., 2013; Strauss et al., 2013). Thus, the  
9 current study of Yedoma and thermokarst deposits is representative for an area covered by  
10 similar permafrost deposits of late Pleistocene and Holocene age.

### 11 **4.1 Sediment facies**

12 The grain-size distribution curves (Fig. 2, S1) indicate a constant deposition environment for  
13 the Yedoma sequences. According to Strauss et al. (2012), there have been stable deposition  
14 conditions during Yedoma accumulation; this hypothesis is supported by the data presented  
15 here. The three thermokarst profiles include three different kinds of thermokarst deposits.  
16 Buo-05 is dominated by a lake facies containing valves of two freshwater ostracod taxa:  
17 *Cytherissa lacustris* and *Cypria* sp. Moreover, shells have been found in Buo-05 (Strauss and  
18 Schirrmeister, 2011). An ice wedge is located next to Buo-01, which points to sub-aerial  
19 conditions like a polygon mire. Buo-03 is interpreted as initial thermokarst on top of a  
20 Yedoma hill. Thus, the grain-size distributions of Buo-05 and Buo-01 reveal that the  
21 thermokarst is granulometrically composed of the same material as Yedoma. The grain-size  
22 distributions in Buo-03 paint a different picture. This distribution is likely caused by the early  
23 state of thermokarst development dominated by peat aggradation. This peat can act like a  
24 selective sediment trap influencing the grain-size distributions, e.g. by producing a less  
25 distinct coarse silt-fine sand peak.

### 26 **4.2 Organic matter degradation**

27 The organic matter proxies of Yedoma deposits are less variable than those of thermokarst  
28 deposits (Buo-01 and 03). Except for the paleocryosols, the cryopedolith parts of the Yedoma  
29 and the Buo-05 thermokarst profile reveal a rather homogenous picture (Fig. 3, 4, S5, S6).  
30 Constant grain-size distributions, less TOC<sub>wt%</sub>, and smaller absolute lipid concentration

1 scattering reveal that the OC stored in the Yedoma deposits has likely been kept perennially  
2 frozen since incorporation. The organic matter signatures (Fig. 4, S2, and S3) as well as the  
3 grain-size distributions (Fig. 2, S1) of thermokarst deposits, especially in Buo-01 and Buo-03,  
4 show broader variations. This is caused by a more complex degradation and re-deposition  
5 history due to reworking. The degradation markers of organic matter found in the  
6 paleocryosol parts of all profiles reveal a less-degraded state, indicating that the organic  
7 matter in these portions is the best preserved.

8 The mean  $\text{TOC}_{\text{wt}\%}$  content for Yedoma deposits is comparable to other sites (Fig. S7) in the  
9 Yedoma region (Schirrmeister et al., 2011b; Schirrmeister et al., 2013). Intense accumulation  
10 and frozen preservation of plant remains ( $14 \text{ kgC/m}^3$  for Yedoma and  $24 \text{ kgC/m}^3$  for  
11 thermokarst deposits) is caused by syngenetic permafrost formation in polygonal tundra  
12 landscapes over long periods in the Quaternary (Schirrmeister et al., 2013). But comparing the  
13 studied deposits to the overall Yedoma region mean ( $19 \text{ kgC/m}^3$  for Yedoma deposits and  $33$   
14  $\text{kgC/m}^3$  (disregarding wedge-ice content) for thermokarst deposits, Strauss et al. (2013)) on  
15 Buor Khaya Peninsula reveals that both deposit types contain less OC. Nevertheless, these  
16 numbers show that such deposits comprise a large pool of dormant carbon, which could be  
17 reactivated due to permafrost thawing. Moreover, thermokarst deposits seem to be the  
18 quantitatively more important OC pool (Yedoma : thermokarst carbon ratio  $\sim 2:3$ ). The higher  
19 carbon inventory in thermokarst deposits is partially related to a concentration effect for  
20 reworked Yedoma OC due to thaw subsidence progression including ground ice loss plus  
21 input of Holocene OC. Together with ecosystem recovery, thermokarst basins can act as a  
22 local sink for portions of the carbon released from thawing permafrost deposits (van  
23 Huissteden and Dolman, 2012). Nevertheless, at the same time thermokarst lakes also  
24 promote intense organic matter degradation including methane production in the anaerobic  
25 environments of organic-rich lake sediments and unfrozen deposits (Walter et al., 2007b;  
26 Shirokova et al., 2013). To answer this question arisen in the introduction, if the thermokarst  
27 organic matter pool is as degradable as the frozen late Pleistocene Yedoma we visualized the  
28 stratigraphically differentiated main proxies in Fig. 7.

29 In our study the C/N data shows an overlap (Fig. 7b). The average values are relatively close  
30 together for all profiles, but the differences are statistically significant (Tab. S1). Thus, the  
31 C/N medians and means hint at a lower degradation state/better organic matter quality of  
32 thermokarst deposits (especially Buo-01 and Buo-03). Moreover, in both Yedoma and

1 thermokarst deposits the same pattern is visible: A positive linear relationship exists between  
2  $\text{TOC}_{\text{wt}\%}$  and C/N ratios (Fig. 5b). In soil science literature it is agreed that the elemental  
3 composition of organic matter is affected by the degree of humification and microbial  
4 activities that metabolize the organic matter (Kumada, 1987). Ongoing organic-matter  
5 decomposition will release stored C to the atmosphere and N to the soil (Weintraub and  
6 Schimel, 2005), resulting in a lower C/N ratio for more-degraded deposits (Gundelwein et al.,  
7 2007). This was found in (sub-) arctic peat deposits and soils, where the C/N ratio decreases  
8 with depth (Kuhry and Vitt, 1996; McKane et al., 1997; Ping et al., 1998). Because a high TN  
9 content can promote stabilization of organic matter at late stages of decomposition (Berg,  
10 2000), this further supports the interpretation that a low C/N ratio indicates  
11 recalcitrant/matured organic matter (Rumpel and Kögel-Knabner, 2011). Schädel et al. (2014)  
12 found, with incubation studies, that the C/N ratio is a good estimator for organic-matter  
13 decomposability/vulnerability. Although the C/N ratios are lower than in arctic peat deposits  
14 (Hugelius et al., 2012; Routh et al., 2014), the ratios are still in the range of or higher than  
15 those found in many other deep mineral soils of the temperate zone (Jenkinson et al., 2008;  
16 Rumpel and Kögel-Knabner, 2011). Thus, both Yedoma and thermokarst deposits show  
17 relatively good organic matter quality for microbial decay after becoming available by thaw.  
18 The C/N ratios, especially for the paleocryosols, suggest that good quality organic matter was  
19 preserved (by sub- or near 0°C temperatures during thermokarst processes) for future  
20 decomposition. This is shown by the  $\delta^{13}\text{C}$  ratio as well. Neglecting the influence of different  
21 sources of organic matter on the  $\delta^{13}\text{C}$  ratio, which is justified by constant ACL values of >28  
22 (higher land plants, Fig. S4) for Yedoma and thermokarst deposits, the  $\delta^{13}\text{C}$  ratio is an  
23 appropriate proxy to use to estimate the intrinsic state of degradation. Therefore, the  $\delta^{13}\text{C}$   
24 indicate a significant lower organic matter degradation for the thermokarst samples, implying  
25 a better quality than that found in Yedoma samples. The high CPI values of the thermokarst  
26 and the Yedoma organic matter (around 9 and higher) indicate fresh and less degraded  
27 terrigenous organic matter (Brassell et al., 1978) for both deposits (Fig. 7d). The even  
28 (significantly) higher CPI values of the Yedoma deposit organic matter indicate a better  
29 quality for further decomposition (Fig. 7d) than in the thermokarst deposits.

30 Routh et al. (2014) states that other, more labile compounds like *n*-alcohols and *n*-fatty acids  
31 are degraded to *n*-alkanes. Thus, an increase of *n*-alkanes (Fig. 3 and 4, absolute lipid  
32 concentration column) is an indicator for cumulative decay. We do not see a decreasing trend,  
33 which points to a constant low decomposition state. In addition, no increasing *n*-fatty acid CPI

1 with depth (as was shown in an arctic peat by Andersson and Meyers (2012)) was obvious.  
2 (Andersson and Meyers, 2012) interpreted this to reflect fatty acid production during  
3 humification, but we do not see this humification effect in our data, either in Yedoma, or in  
4 the thermokarst deposits. Moreover, as indicated by the dominance of long-chain *n*-alkane  
5 and *n*-fatty-acid compounds vs. compounds of shorter chain length (Höfle et al., 2013), we  
6 confirm the interpretation of good organic matter preservation in both Yedoma and  
7 thermokarst deposits. At first view, the hop-17(21)-ene (Fig. 7e) concentration does not show  
8 a significant preservation difference between both kinds of deposits, because the Buo-04  
9 Yedoma profile contains hopene concentrations in the same range as those found in  
10 thermokarst deposits. However, if we focus on the median values, the Yedoma deposits again  
11 appear to be slightly more strongly degraded than the thermokarst deposits. With the  
12 exception of Buo-01, the HPFA index (Fig. 7f) also suggests lower degradation and better  
13 organic matter quality in the thermokarst deposit profiles (Buo-05 and Buo-03). Our HPFA  
14 index, introduced based on Poynter's (1989) HPA index which was tested in the Arctic  
15 environment by Routh et al. (2014), is an appropriate indicator of the relative amount of the  
16 labile fatty acids that remain in a sample. The uppermost samples just below the surface at  
17 Buo-04, Buo-05, and Buo-01 with lower HPFA values are clearly an exception and suggest  
18 the entrainment of higher proportions of material influenced by Holocene degradation. This is  
19 likely caused by the fairly recent influence of an active layer or transient layer and warmer  
20 permafrost temperatures. The Oleanen ratio shows a separation of Yedoma and thermokarst  
21 deposits, but this ratio is dominated by numerous 0.0 measurements in the Yedoma deposits.  
22 These results might be caused not only by transformation of  $\beta$ -amyrin to Olean-12-ene (by  
23 losing the hydroxyl group) or to Olean-13(18)-ene (by losing the double bond), but also by so  
24 far unknown processes in the Yedoma deposits. Thus, because of sparse data, we interpret this  
25 proxy as a better Yedoma organic matter quality for further decomposition.

26 Summing up Fig. 7, thermokarst organic matter is partly less degraded compared to the  
27 organic matter sequestered in Yedoma deposits (see table S1, significance for C/N,  $\delta^{13}\text{C}$ , and  
28 the HPFA index). The CPI points in the other direction (Fig. 7 and table S1). For hop-17(21)-  
29 ene, we do not see significant differences. Nevertheless, the interquartile ranges show an  
30 overlap for most proxies. We interpret this as following: Compared to unaltered Yedoma  
31 deposits, degradation during thermokarst processes, but also heightened amounts of OC input  
32 during climatically more favorable Holocene times, are balancing each other concerning the  
33 organic matter quality for future degradation. Nevertheless, as there is more carbon stored in

1 the thermokarst basins (Strauss et al. 2013), thermokarst deposits imply a higher intrinsic  
2 potential to contribute greenhouse gases in a warmer future. This is supported by the acetate  
3 data indicating a higher mean content for the thermokarst deposits. Acetate is an excellent  
4 substrate for microbial turnover e.g. acetoclastic methanogenesis (Kotsyurbenko et al.,  
5 2004). The PCA confirms the picture of little difference between the organic matter  
6 preservation of the Yedoma and the thermokarst samples. Especially Fig. 6a, supported by  
7 Fig. 2, reveals that Yedoma and thermokarst are composed of similar sediments. The Buo-05  
8 thermokarst profile is very similar to both Yedoma profiles. The PCA of the degradation  
9 proxies (Fig. 6b) also shows no clusters, but exhibits slightly better separation between both  
10 kinds of deposits. Fig. 6b reveals that the C/N ratio, the  $\delta^{13}\text{C}$  ratio, and the CPI are correlated.  
11 This is also separately illustrated in Fig. 5a and c. Thus, these proxies seem to confirm each  
12 other. The PCA of the *n*-alkane chain length points to a potential dominance of longer chain  
13 alkanes in Yedoma and shorter chain alkanes in thermokarst, indicating better quality for  
14 further decomposition of Yedoma samples (Höfle et al., 2013). Exceptions are the Buo-05-A-  
15 01 and Buo-03-A-03 thermokarst samples which point in the same direction as the *n*-C<sub>35</sub>  
16 concentration.

17 The abovementioned overlap of the interquartile range (Fig. 7) and especially the PCA of the  
18 biomarkers (Fig. 6b and c) show that the organic matter degradation/decomposition  
19 vulnerability is heterogeneous and depends on different decomposition trajectories and  
20 differing former decomposition/incorporation histories. This is likely shown in both Yedoma  
21 and thermokarst deposits, covering the whole range of degradation proxy values (Fig 7b, c, e).  
22 To elucidate this was one of the benefits of the applied multiproxy approach. With the  
23 addition of biomarker data, it is possible to show that the permafrost organic matter  
24 degradation is not a linear function of age or sediment facies, but likely a combination of  
25 (interrupted) degradation cycles and a cascade of degradation steps. In particular, the  
26 reasonably good organic matter preservation of thermokarst deposits reveals that the sediment  
27 degradation processes do not necessarily degrade the organic matter. Potentially, the loss of  
28 labile OC during thermokarst processes was compensated for by high rates of Holocene OC  
29 accumulation in e.g. lake sediments. Nutrient release from thawing permafrost could have  
30 stimulated lake productivity, whereas decomposition was slow because of low lake  
31 temperatures, resulting in cold anoxic lake environments (Boike et al., 2013; Walter Anthony  
32 et al., 2014). When the lake drained, permafrost formation rapidly recovered the sediments  
33 (Jones et al., 2011) including any possibly newly-accumulated OC.

### 1 **4.3 Fate of organic matter**

2 The permafrost OC resilience or vulnerability is a topic of recent research (Schuur and  
3 Abbott, 2011; Knoblauch et al., 2013; Hodgkins et al., 2014; Li et al., 2014; Mu et al., 2014).  
4 Any warming permafrost is potentially vulnerable to thawing. The remaining important  
5 question is this: What is the fate of the organic matter exposed to degradation after permafrost  
6 has thawed? The lipid biomarker data discussed (CPI etc.) indicates that the organic matter in  
7 the sediments was, after initial degradation processes, relatively quickly protected against  
8 microbial alteration by freezing. This is confirmed by an absent degradation - depth trend  
9 which reveals good organic matter quality independent of age. Thus, the very old frozen  
10 organic matter is also vulnerable to degradation after thawing. This interpretation fits results  
11 from studies of permafrost-affected Arctic peats (Hugelius et al., 2012; Routh et al., 2014).  
12 Walter Anthony et al. (2014) found a net accumulation in thermokarst basins since the last  
13 deglaciation, but predict a change to a large carbon source when permafrost thaws and the OC  
14 will be available for oxidation. Due to ongoing climate warming in the Arctic, Grosse et al.  
15 (2011b) suppose an increasing occurrence and magnitude of disturbance processes, especially  
16 fire and thermokarst, which will accelerate permafrost degradation. Because our  
17 sedimentological and biomarker proxies show a low degradation state, especially for the  
18 paleocryosol sequences, we expect a significant vulnerability to microbial degradation after  
19 thawing. As evidence that the OC is vulnerable when thawed, Gaglioti et al. (2014) found that  
20 ~10 times more ancient OC found in permafrost was made available for degradation during  
21 warm times of the Holocene (Holocene Thermal Maximum (11.7-9.0 ka) and Bølling-Allerød  
22 periods) than is available today. By increased disturbances like deep surface subsidence  
23 caused by thawing and the draining of excess water from melting ice in a warmer climate, the  
24 Yedoma and, to a lesser degree because of lower excess ice content, the thermokarst organic  
25 matter could become deeply bioavailable. The wedge-ice volume is estimated at up to ~60  
26 vol% for Yedoma and up to ~10 vol% for thermokarst deposits (Ulrich et al., 2014). When  
27 added to segregated ice, ~80 vol% and ~65 vol% mean sedimentary ice volume exists in  
28 Yedoma and thermokarst, respectively (Strauss et al., 2013). When it becomes available and  
29 is exported as dissolved OC to e.g. river systems, Vonk et al. (2013) and Mann et al. (2014)  
30 found that dissolved OC (<0.45  $\mu\text{m}$ ) in ancient Yedoma is exceptionally biolabile. But if it is  
31 not dissolved, the suspended (>0.45  $\mu\text{m}$ ) eroded ancient organic matter could be protected  
32 from extensive degradation by organo-mineral bonds, which stabilize the organic matter

1 (Höfle et al., 2013) and, in an aquatic environment, promote rapid settling because they weigh  
2 down the organic matter (Vonk et al., 2010).

3 From the modeling perspective, global-scale models are limited so far because they  
4 implement one-dimensional vertical thaw only (Koven et al., 2011; Schneider von Deimling  
5 et al., 2012; Schaphoff et al., 2013). Thus, the potentially labile Yedoma and thermokarst  
6 deep OC pool described in this study is not realistically implemented in these models, because  
7 the models disregard rapid phenomena like thermokarst processes. Thermokarst processes,  
8 despite being local in nature, are widespread on the regional scale (Grosse et al., 2011a) and  
9 may constitute the crucial process making the deep OC studied here microbiologically  
10 available.

## 11 **5 Conclusions**

12 As being freeze-locked, the great amount of organic matter in the studied sediments is highly  
13 decomposable. Generally, in all applied proxies there is no degradation - depth trend obvious,  
14 revealing that permafrost acts like a freezer, preserving the organic matter after freezing.  
15 Based on interpreting the mean values of the C/N ratio, isotope ratio ( $\delta^{13}\text{C}$ ), and the HPFA  
16 index, the thermokarst organic matter is less degraded and of better quality for degradation  
17 after thawing compared to the organic matter sequestered in Yedoma deposits. The CPI data  
18 suggest less degradation of the organic matter from both deposits with a higher value for  
19 Yedoma organic matter. For the hop-17(21)-ene concentration no significant difference was  
20 found. We do not see any conflict between these two determinations, because the interquartile  
21 ranges overlap for most proxies. We interpret this to indicate a comparable magnitude of  
22 organic matter quality in both kinds of deposits, but with a likely better thermokarst organic  
23 matter quality for further degradation. For a modelling approach, this conclusion could be  
24 extrapolated to the Laptev Sea Region as the studied deposits are akin to other Yedoma and  
25 thermokarst deposits of the northeast Siberian Arctic (Schirrmeister et al. 2011a).

26 The fate of mobilized Yedoma deposit OC depends largely on the environmental conditions  
27 that exist during the thermokarst processes and in the resulting thermokarst basin. In  
28 conclusion, when the conditions are good for organic matter preservation, for example cold  
29 (slightly above 0°C) or anoxic (lake) conditions, and reworked fossil organic matter can  
30 rapidly refreeze to permafrost, good-quality organic matter for further decomposition can be  
31 maintained and inputs likely compensate for losses due to thermokarst degradation.

32

## 1 **Author contribution**

2 J. Strauss, L. Schirrmeister, and S. Wetterich sampled and coordinated all sediment sampling  
3 at the Buor Khaya field campaign in 2010. K. Mangelsdorf supported the biomarker analysis  
4 and interpretation. J. Strauss carried out the laboratory analyses, except for one profile, which  
5 was analyzed by L. Eichhorn. U. Herzsuh designed the statistical analyses. J. Strauss  
6 planned and wrote the publication with input from all co-authors.

## 7 **Acknowledgements**

8 We acknowledge support of this research by the German Ministry of Education and Research  
9 (the "System Laptev Sea" and "CarboPerm" (03G0836A) projects). We also thank the  
10 Russian and German partners who were involved in the "Eastern Laptev Sea - Buor Khaya  
11 Peninsula 2010" expedition. J. Strauss was supported by a grant by the Studienstiftung des  
12 deutschen Volkes (German National Academic Foundation) and a European Research  
13 Council Starting Grant (PETA-CARB, #338335).

## 14 **References**

15 Andersson, R. A., Kuhry, P., Meyers, P., Zebühr, Y., Crill, P., and Mörth, M.: Impacts of  
16 paleohydrological changes on n-alkane biomarker compositions of a holocene peat sequence  
17 in the eastern European Russian Arctic, *Organic Geochemistry*, 42, 1065-1075,  
18 doi:10.1016/j.orggeochem.2011.06.020, 2011.

19 Andersson, R. A., and Meyers, P. A.: Effect of climate change on delivery and degradation of  
20 lipid biomarkers in a Holocene peat sequence in the eastern European Russian Arctic, *Organic*  
21 *Geochemistry*, 53, 63-72, doi:10.1016/j.orggeochem.2012.05.002, 2012.

22 Berg, B.: Litter decomposition and organic matter turnover in northern forest soils, *Forest*  
23 *Ecology and Management*, 133, 13-22, doi:10.1016/S0378-1127(99)00294-7, 2000.

24 Blott, S. J., and Pye, K.: Gradistat: A grain size distribution and statistics package for the  
25 analysis of unconsolidated sediments, *Earth Surface Processes and Landforms*, 26, 1237-  
26 1248, doi:10.1002/esp.261, 2001.

27 Boike, J., Kattenstroth, B., Abramova, K., Bornemann, N., Chetverova, A., Fedorova, I.,  
28 Fröb, K., Grigoriev, M., Grüber, M., Kutzbach, L., Langer, M., Minke, M., Muster, S., Piel,  
29 K., Pfeiffer, E. M., Stoof, G., Westermann, S., Wischnewski, K., Wille, C., and Hubberten, H.  
30 W.: Baseline characteristics of climate, permafrost and land cover from a new permafrost



1 observatory in the Lena River Delta, Siberia (1998-2011), *Biogeosciences*, 10, 2105-2128,  
2 doi:10.5194/bg-10-2105-2013, 2013.

3 Brassell, S., Eglinton, G., Maxwell, J., and Philp, R.: Natural background of alkanes in the  
4 aquatic environment. In: *Aquatic pollutants: Transformation and biological effects*, Hutzinger,  
5 O., Lelyveld, I. H., and Zoetman, B. C. J. (Eds.), Pergamon Press, Oxford, 1978.

6 Bray, E. E., and Evans, E. D.: Distribution of n-paraffins as a clue to recognition of source  
7 beds, *Geochimica et Cosmochimica Acta*, 22, 2-15, doi:10.1016/0016-7037(61)90069-2,  
8 1961.

9 Ciais, P., Tagliabue, A., Cuntz, M., Bopp, L., Scholze, M., Hoffmann, G., Lourantou, A.,  
10 Harrison, S. P., Prentice, I. C., Kelley, D. I., Koven, C., and Piao, S. L.: Large inert carbon  
11 pool in the terrestrial biosphere during the last glacial maximum, *Nature Geoscience*, 5, 74-  
12 79, doi:10.1038/ngeo1324, 2012.

13 Dlugokencky, E., and Tans, P.: Trends in atmospheric carbon dioxide:  
14 <http://www.esrl.noaa.gov/gmd/ccgg/trends/global.html>, access: 23.03.2014, 2014.

15 Drachev, S. S., Savostin, L. A., Groshev, V. G., and Bruni, I. E.: Structure and geology of the  
16 continental shelf of the Laptev Sea, eastern Russian Arctic, *Tectonophysics*, 298, 357-393,  
17 doi:10.1016/S0040-1951(98)00159-0, 1998.

18 Drozdov, D. S., Rivkin, F. M., Rachold, V., Ananjeva-Malkova, G. V., Ivanova, N. V.,  
19 Chehina, I. V., Koreisha, M. M., Korostelev, Y. V., and Melnikov, E. S.: Electronic atlas of  
20 the Russian Arctic coastal zone, *Geo-Marine Letters*, 25, 81-88, doi:10.1007/s00367-004-  
21 0189-7, 2005.

22 Folk, R. L., and Ward, W. C.: Brazos river bar: A study in the significance of grain size  
23 parameters, *Journal of Sedimentary Petrology*, 27, 3-26, 1957.

24 Gaglioti, B. V., Mann, D. H., Jones, B. M., Pohlman, J. W., Kunz, M. L., and Wooller, M. J.:  
25 Radiocarbon age-offsets in an Arctic lake reveal the long-term response of permafrost carbon  
26 to climate change, *Journal of Geophysical Research: Biogeosciences*, 119, 1630–1651,  
27 doi:10.1002/2014jg002688, 2014.

28 Glombitza, C., Mangelsdorf, K., and Horsfield, B.: Maturation related changes in the  
29 distribution of ester bound fatty acids and alcohols in a coal series from the New Zealand coal

1 band covering diagenetic to catagenetic coalification levels, *Organic Geochemistry*, 40, 1063-  
2 1073, doi:10.1016/j.orggeochem.2009.07.008, 2009.

3 Goslar, T., Czernik, J., and Goslar, E.: Low-energy <sup>14</sup>C AMS in Poznań radiocarbon laboratory,  
4 Poland, *Nuclear Instruments and Methods in Physics Research Section B: Beam Interactions*  
5 *with Materials and Atoms*, 223–224, 5-11, doi:10.1016/j.nimb.2004.04.005, 2004.

6 Grosse, G., Harden, J., Turetsky, M. R., McGuire, A. D., Camill, P., Tarnocai, C., Frolking,  
7 S., Schuur, E. A. G., Jorgenson, T., Marchenko, S., Romanovsky, V., Wickland, K. P.,  
8 French, N., Waldrop, M. P., Bourgeau-Chavez, L., and Striegl, R. G.: Vulnerability of high-  
9 latitude soil organic carbon in North America to disturbance, *Journal of Geophysical*  
10 *Research*, 116, G00K06, doi:10.1029/2010JG001507, 2011a.

11 Grosse, G., Romanovsky, V., Jorgenson, T., Anthony, K. W., Brown, J., and Overduin, P. P.:  
12 Vulnerability and feedbacks of permafrost to climate change, *Eos, Transactions American*  
13 *Geophysical Union*, 92, 73-74, doi:10.1029/2011eo090001, 2011b.

14 Grosse, G., Robinson, J. E., Bryant, R., Taylor, M. D., Harper, W., DeMasi, A., Kyker-  
15 Snowman, E., Veremeeva, A., Schirrmeister, L., and Harden, J.: Distribution of late  
16 Pleistocene ice-rich syngenetic permafrost of the yedoma suite in east and central Siberia,  
17 Russia, U.S. Geological Survey Open File Report, 1078, U.S. Geological Survey, Reston,  
18 USA, 37 pp, 2013.

19 Gubin, S. V., and Veremeeva, A. A.: Parent materials enriched in organic matter in the  
20 northeast of Russia, *Eurasian Soil Science*, 43, 1238-1243, doi:10.1134/s1064229310110062,  
21 2010.

22 Gundelwein, A., Muller-Lupp, T., Sommerkorn, M., Haupt, E. T. K., Pfeiffer, E., and  
23 Wiechmann, H.: Carbon in tundra soils in the lake labaz region of Arctic Siberia, *European*  
24 *Journal of Soil Science*, 58, pp. 1164-1174, 2007.

25 Günther, F., Overduin, P. P., Sandakov, A., Grosse, G., and Grigoriev, M. N.: Thermo-  
26 erosion along the yedoma coast of the Buor Khaya peninsula, Laptev Sea, east Siberia,  
27 *Proceedings of the Tenth International Conference on Permafrost, Volume 1: International*  
28 *Contributions, Salekhard, Russia, 25-29 June 2012*, 137-142, 2012

29 Günther, F., Overduin, P. P., Sandakov, A. V., Grosse, G., and Grigoriev, M. N.: Short- and  
30 long-term thermo-erosion of ice-rich permafrost coasts in the Laptev Sea region,  
31 *Biogeosciences*, 10, 4297-4318, doi:10.5194/bg-10-4297-2013, 2013.

1 Heyer, J., Hübner, H., and Maaß, I.: Isotopenfraktionierung des Kohlenstoffs bei der  
2 mikrobiellen Methanbildung, *Isotopes in Environmental and Health Studies*, 12, 202–205,  
3 doi:10.1080/10256017608543912, 1976.

4 Hodgkins, S. B., Tfaily, M. M., McCalley, C. K., Logan, T. A., Crill, P. M., Saleska, S. R.,  
5 Rich, V. I., and Chanton, J. P.: Changes in peat chemistry associated with permafrost thaw  
6 increase greenhouse gas production, *Proceedings of the National Academy of Sciences*, 111,  
7 5819-5824, doi:10.1073/pnas.1314641111, 2014.

8 Höfle, S., Rethemeyer, J., Mueller, C. W., and John, S.: Organic matter composition and  
9 stabilization in a polygonal tundra soil of the Lena Delta, *Biogeosciences*, 10, 3145-3158,  
10 doi:10.5194/bg-10-3145-2013, 2013.

11 Hugelius, G., Routh, J., Kuhry, P., and Crill, P.: Mapping the degree of decomposition and  
12 thaw remobilization potential of soil organic matter in discontinuous permafrost terrain,  
13 *Journal of Geophysical Research: Biogeosciences*, 117, G02030, doi:10.1029/2011jg001873,  
14 2012.

15 Hugelius, G., Strauss, J., Zubrzycki, S., Harden, J., Schuur, E. A. G., Ping, C.-L.,  
16 Schirrmeister, L., Grosse, G., Michaelson, G., Koven, C., O'Donnel, J., Elberling, B., Mishra,  
17 U., Camill, P., Yu, Z., Palmtag, J., and Kuhry, P.: Estimated stocks of circumpolar permafrost  
18 carbon with quantified uncertainty ranges and identified data gaps, *Biogeosciences*, 11, 6573–  
19 6593, doi:10.5194/bg-11-6573-2014, 2014.

20 Jenkinson, D. S., Poulton, P. R., and Bryant, C.: The turnover of organic carbon in subsoils.  
21 Part 1. Natural and bomb radiocarbon in soil profiles from the Rothamsted long-term field  
22 experiments, *European Journal of Soil Science*, 59, 391-399, doi:10.1111/j.1365-  
23 2389.2008.01025.x, 2008.

24 Jones, B. M., Grosse, G., Arp, C. D., Jones, M. C., Walter Anthony, K. M., and Romanovsky,  
25 V. E.: Modern thermokarst lake dynamics in the continuous permafrost zone, northern  
26 Seward Peninsula, Alaska, *J. Geophys. Res.*, 116, G00M03, doi:10.1029/2011JG001666,  
27 2011.

28 Knoblauch, C., Beer, C., Sosnin, A., Wagner, D., and Pfeiffer, E.-M.: Predicting long-term  
29 carbon mineralization and trace gas production from thawing permafrost of northeast Siberia,  
30 *Glob. Change Biol.*, 19, 1160–1172, doi:10.1111/gcb.12116, 2013.

1 Kotsyurbenko, O. R., Chin, K.-J., Glagolev, M. V., Stubner, S., Simankova, M. V.,  
2 Nozhevnikova, A. N., and Conrad, R.: Acetoclastic and hydrogenotrophic methane  
3 production and methanogenic populations in an acidic West-Siberian peat bog, *Environmental*  
4 *Microbiology*, 6, 1159-1173, doi:10.1111/j.1462-2920.2004.00634.x, 2004.

5 Koven, C. D., Ringeval, B., Friedlingstein, P., Ciais, P., Cadule, P., Khvorostyanov, D.,  
6 Krinner, G., and Tarnocai, C.: Permafrost carbon-climate feedbacks accelerate global  
7 warming, *Proceedings of the National Academy of Sciences*, 108, 14769-14774,  
8 doi:10.1073/pnas.1103910108, 2011.

9 Kuesel, K., and Drake, H. L.: Effects of environmental parameters on the formation and  
10 turnover of acetate by forest soils, *Applied and environmental microbiology*, 61, 3667-3675,  
11 1995.

12 Kuhry, P., and Vitt, D. H.: Fossil carbon/nitrogen ratios as a measure of peat decomposition,  
13 *Ecology*, 77, 271-275, doi:10.2307/2265676, 1996.

14 Kuhry, P., Ping, C.-L., Schuur, E. A. G., Tarnocai, C., and Zimov, S.: Report from the  
15 international permafrost association: Carbon pools in permafrost regions, *Permafrost*  
16 *Periglacial Process.*, 20, 229-234, doi:10.1002/ppp.648, 2009.

17 Kumada, K.: Chemistry of soil organic matter, *Developments in soil science*, Elsevier/Japan  
18 Scientific Societies Press, Amsterdam, 1987.

19 Lee, H., Schuur, E. A. G., Inglett, K. S., Lavoie, M., and Chanton, J. P.: The rate of  
20 permafrost carbon release under aerobic and anaerobic conditions and its potential effects on  
21 climate, *Glob. Change Biol.*, 18, 515-527, doi:10.1111/j.1365-2486.2011.02519.x, 2012.

22 Li, J., Luo, Y., Natali, S., Schuur, E. A. G., Xia, J., Kowalczyk, E., and Wang, Y.: Modeling  
23 permafrost thaw and ecosystem carbon cycle under annual and seasonal warming at an Arctic  
24 tundra site in Alaska, *Journal of Geophysical Research: Biogeosciences*, 119, 2013JG002569,  
25 doi:10.1002/2013jg002569, 2014.

26 Luo, Q., Yu, S., Liu, Y., Zhang, Y., Han, H., Qi, L., and Zhong, N.: Existence and  
27 implications of hop-17(21)-enes in the lower cretaceous of the Saihantala Sag, Erlian Basin,  
28 China, *Pet. Sci.*, 9, 154-160, doi:10.1007/s12182-012-0195-8, 2012.

29 Mangelsdorf, K., Finsel, E., Liebner, S., and Wagner, D.: Temperature adaptation of  
30 microbial communities in different horizons of Siberian permafrost-affected soils from the

1 Lena Delta, *Chemie der Erde - Geochemistry*, 69, 169-182,  
2 doi:10.1016/j.chemer.2009.02.001, 2009.

3 Mann, P. J., Sobczak, W. V., LaRue, M. M., Bulygina, E., Davydova, A., Vonk, J. E., Schade,  
4 J., Davydov, S., Zimov, N., Holmes, R. M., and Spencer, R. G. M.: Evidence for key  
5 enzymatic controls on metabolism of Arctic river organic matter, *Glob. Change Biol.*, 20,  
6 1089-1100, doi:10.1111/gcb.12416, 2014.

7 Marzi, R., Torkelson, B. E., and Olson, R. K.: A revised carbon preference index, *Organic*  
8 *Geochemistry*, 20, 1303-1306, doi:10.1016/0146-6380(93)90016-5, 1993.

9 McKane, R. B., Rastetter, E. B., Shaver, G. R., Nadelhoffer, K. J., Giblin, A. E., Laundre, J.  
10 A., and Chapin, F. S.: Climatic effects on tundra carbon storage inferred from experimental  
11 data and a model, *Ecology*, 78, 1170-1187, doi:10.1890/0012-  
12 9658(1997)078[1170:ceotcs]2.0.co;2, 1997.

13 Mu, C., Zhang, T., Schuster, P. F., Schaefer, K., Wickland, K. P., Repert, D. A., Liu, L.,  
14 Schaefer, T., and Cheng, G.: Carbon and geochemical properties of cryosols on the north  
15 slope of Alaska, *Cold Regions Science and Technology*, 100, 59-67,  
16 doi:10.1016/j.coldregions.2014.01.001, 2014.

17 Oksanen, J.: *Multivariate analysis of ecological communities in r: Vegan tutorial*, University  
18 of Oulu, Oulu, 43 pp., 2013.

19 Ping, C. L., Bockheim, J. G., Kimble, J. M., Michaelson, G. J., and Walker, D. A.:  
20 Characteristics of cryogenic soils along a latitudinal transect in Arctic Alaska, *Journal of*  
21 *Geophysical Research: Atmospheres*, 103, 28917-28928, doi:10.1029/98jd02024, 1998.

22 Poynter, J., and Eglinton, G.: 14. Molecular composition of three sediments from hole 717c:  
23 The Bengal fan, *Proceedings of the Ocean Drilling Program: Scientific results*, 116, 155-161,  
24 1990.

25 Poynter, J.: *Molecular stratigraphy: The recognition of palaeoclimatic signals in organic*  
26 *geochemical data*, PhD, School of Chemistry, University of Bristol, Bristol, 324 pp., 1989.

27 Radke, M., Willsch, H., and Welte, D. H.: Preparative hydrocarbon group type determination  
28 by automated medium pressure liquid chromatography, *Analytical Chemistry*, 52, 406-411,  
29 doi:10.1021/ac50053a009, 1980.

- 1 Romanovskii, N. N., Hubberten, H. W., Gavrilov, A. V., Tumskey, V. E., and Kholodov, A.  
2 L.: Permafrost of the east Siberian Arctic shelf and coastal lowlands, *Quaternary Science*  
3 *Reviews*, 23, 1359-1369, doi:10.1016/j.quascirev.2003.12.014, 2004.
- 4 Romanovsky, V. E., Smith, S. L., and Christiansen, H. H.: Permafrost thermal state in the  
5 polar northern hemisphere during the international polar year 2007–2009: A synthesis,  
6 *Permafrost Periglacial Process.*, 21, 106-116, doi:10.1002/ppp.689, 2010.
- 7 Routh, J., Hugelius, G., Kuhry, P., Filley, T., Tillman, P. K., Becher, M., and Crill, P.: Multi-  
8 proxy study of soil organic matter dynamics in permafrost peat deposits reveal vulnerability  
9 to climate change in the European Russian Arctic, *Chemical Geology*, 368, 104-117,  
10 doi:10.1016/j.chemgeo.2013.12.022, 2014.
- 11 Rumpel, C., and Kögel-Knabner, I.: Deep soil organic matter - a key but poorly understood  
12 component of terrestrial C cycle, *Plant Soil*, 338, 143-158, doi:10.1007/s11104-010-0391-5,  
13 2011.
- 14 Schädel, C., Schuur, E. A. G., Bracho, R., Elberling, B., Knoblauch, C., Lee, H., Luo, Y. Q.,  
15 Shaver, G. R., and Turetsky, M. R.: Circumpolar assessment of permafrost C quality and its  
16 vulnerability over time using long-term incubation data, *Glob. Change Biol.*, 20, 641-652,  
17 doi:10.1111/gcb.12417, 2014.
- 18 Schaphoff, S., Heyder, U., Ostberg, S., Gerten, D., Heinke, J., and Lucht, W.: Contribution of  
19 permafrost soils to the global carbon budget, *Environmental Research Letters*, 8, 014026,  
20 doi:10.1088/1748-9326/8/1/014026, 2013.
- 21 Schirrmeister, L., Grosse, G., Wetterich, S., Overduin, P. P., Strauss, J., Schuur, E. A. G., and  
22 Hubberten, H.-W.: Fossil organic matter characteristics in permafrost deposits of the northeast  
23 Siberian Arctic, *Journal of Geophysical Research*, 116, G00M02, doi:10.1029/2011jg001647,  
24 2011a.
- 25 Schirrmeister, L., Kunitsky, V., Grosse, G., Wetterich, S., Meyer, H., Schwamborn, G.,  
26 Babiy, O., Derevyagin, A., and Siegert, C.: Sedimentary characteristics and origin of the late  
27 pleistocene ice complex on north-east Siberian Arctic coastal lowlands and islands - a review,  
28 *Quaternary International*, 241, 3-25, doi:10.1016/j.quaint.2010.04.004, 2011b.
- 29 Schirrmeister, L., Froese, D. G., Tumskey, V., Grosse, G., and Wetterich, S.: Yedoma: late  
30 Pleistocene ice-rich syngenetic permafrost of Beringia, in: *Encyclopedia of quaternary*

1 sciences, 2 ed., edited by: Elias, S. A., Quaternary glaciation | cold regions landforms,  
2 Elsevier, Amsterdam, 2013.

3 Schneider von Deimling, T., Meinshausen, M., Levermann, A., Huber, V., Frieler, K.,  
4 Lawrence, D. M., and Brovkin, V.: Estimating the near-surface permafrost-carbon feedback  
5 on global warming, *Biogeosciences*, 9, 649-665, cc, 2012.

6 Schulte, S., Mangelsdorf, K., and Rullkötter, J.: Organic matter preservation on the Pakistan  
7 continental margin as revealed by biomarker geochemistry, *Organic Geochemistry*, 31, 1005-  
8 1022, doi:10.1016/S0146-6380(00)00108-X, 2000.

9 Schuur, E. A. G., Vogel, J. G., Crummer, K. G., Lee, H., Sickman, J. O., and Osterkamp, T.  
10 E.: The effect of permafrost thaw on old carbon release and net carbon exchange from tundra,  
11 *Nature*, 459, 556-559, doi:10.1038/nature08031, 2009.

12 Schuur, E. A. G., and Abbott, B.: High risk of permafrost thaw, *Nature*, 480, 32-33,  
13 doi:10.1038/480032a, 2011.

14 Shirokova, L. S., Pokrovsky, O. S., Kirpotin, S. N., Desmukh, C., Pokrovsky, B. G., Audry,  
15 S., and Viers, J.: Biogeochemistry of organic carbon, CO<sub>2</sub>, CH<sub>4</sub>, and trace elements in  
16 thermokarst water bodies in discontinuous permafrost zones of Western Siberia,  
17 *Biogeochemistry*, 113, 573-593, doi:10.1007/s10533-012-9790-4, 2013.

18 Smith, M. R., and Mah, R. A.: Acetate as sole carbon and energy source for growth of  
19 *methanosarcina* strain 227, *Applied and environmental microbiology*, 39, 993-999, 1980.

20 Sollins, P., Spycher, G., and Glassman, C. A.: Net nitrogen mineralization from light- and  
21 heavy-fraction forest soil organic matter, *Soil Biology and Biochemistry*, 16, 31-37,  
22 doi:10.1016/0038-0717(84)90122-6, 1984.

23 Stevenson, F. J.: *Humus chemistry: Genesis, composition, reactions*, John Wiley & Sons,  
24 New York, 1994.

25 Strauss, J., and Schirrmeister, L.: Permafrost sequences of buor khaya peninsula, in: *Reports*  
26 *on polar and marine research - Russian-German cooperation system Laptev Sea: The*  
27 *expedition eastern Laptev Sea-Buor Khaya Peninsula 2010*, edited by: Wetterich, S.,  
28 Overduin, P. P., and Grigoriev, M., Alfred Wegener Institute for Polar and Marine Research,  
29 Bremerhaven, Germany, 35-50, 2011.

- 1 Strauss, J., Schirrmeister, L., Wetterich, S., Borchers, A., and Davydov, S. P.: Grain-size  
2 properties and organic-carbon stock of yedoma ice complex permafrost from the Kolyma  
3 lowland, northeastern Siberia, *Global Biogeochemical Cycles*, 26, GB3003,  
4 doi:10.1029/2011GB004104, 2012.
- 5 Strauss, J., Schirrmeister, L., Grosse, G., Wetterich, S., Ulrich, M., Herzsuh, U., and  
6 Hubberten, H.-W.: The deep permafrost carbon pool of the yedoma region in Siberia and  
7 Alaska, *Geophys. Res. Lett.*, 40, 6165–6170, doi:10.1002/2013GL058088, 2013.
- 8 Stuiver, M., Reimer, P., and Reimer, R.: Calib 6.0, in, <sup>14</sup>C CHRONO Centre, Queens  
9 University Belfast, Belfast, 2010.
- 10 Tieszen, L.: Photosynthesis and respiration in Arctic tundra grasses: Field light intensity and  
11 temperature responses, *Arctic and Alpine Research*, 5, 239-251, 1973.
- 12 Ulrich, M., Grosse, G., Strauss, J., and Schirrmeister, L.: Quantifying wedge-ice volumes in  
13 yedoma and thermokarst basin deposits, *Permafrost Periglacial Process.*, 25, 151–161,  
14 doi:10.1002/ppp.1810, 2014.
- 15 van Huissteden, J., and Dolman, A. J.: Soil carbon in the Arctic and the permafrost carbon  
16 feedback, *Current Opinion in Environmental Sustainability*, 4, 545-551,  
17 doi:10.1016/j.cosust.2012.09.008, 2012.
- 18 Vieth, A., Mangelsdorf, K., Sykes, R., and Horsfield, B.: Water extraction of coals – potential  
19 for estimating low molecular weight organic acids as carbon feedstock for the deep terrestrial  
20 biosphere, *Organic Geochemistry*, 39, 985-991, doi:10.1016/j.orggeochem.2008.02.012,  
21 2008.
- 22 Vonk, J. E., Sánchez-García, L., Semiletov, I., Dudarev, O., Eglinton, T., Andersson, A., and  
23 Gustafsson, Ö.: Molecular and radiocarbon constraints on sources and degradation of  
24 terrestrial organic carbon along the Kolyma paleoriver transect, east Siberian Sea,  
25 *Biogeosciences*, 7, 3153-3166, doi:10.5194/bg-7-3153-2010, 2010.
- 26 Vonk, J. E., Mann, P. J., Davydov, S., Davydova, A., Spencer, R. G. M., Schade, J., Sobczak,  
27 W. V., Zimov, N., Zimov, S., Bulygina, E., Eglinton, T. I., and Holmes, R. M.: High  
28 biolability of ancient permafrost carbon upon thaw, *Geophys. Res. Lett.*, 40, 2689-2693,  
29 doi:10.1002/grl.50348, 2013.



1 Waldrop, M. P., Wickland, K. P., White Iii, R., Berhe, A. A., Harden, J. W., and  
2 Romanovsky, V. E.: Molecular investigations into a globally important carbon pool:  
3 Permafrost-protected carbon in Alaskan soils, *Glob. Change Biol.*, 16, 2543-2554,  
4 doi:10.1111/j.1365-2486.2009.02141.x, 2010.

5 Walter Anthony, K. M., Zimov, S. A., Grosse, G., Jones, M. C., Anthony, P. M., Chapin III,  
6 F. S., Finlay, J. C., Mack, M. C., Davydov, S., Frenzel, P., and Frohling, S.: A shift of  
7 thermokarst lakes from carbon sources to sinks during the Holocene epoch, *Nature*, 511, 452–  
8 456, doi:10.1038/nature13560, 2014.

9 Walter, K. M., Edwards, M. E., Grosse, G., Zimov, S. A., and Chapin, F. S.: Thermokarst  
10 lakes as a source of atmospheric CH<sub>4</sub> during the last deglaciation, *Science*, 318, 633-636,  
11 doi:10.1126/science.1142924, 2007a.

12 Walter, K. M., Smith, L. C., and Chapin, S. F.: Methane bubbling from northern lakes:  
13 Present and future contributions to the global methane budget, *Philosophical Transactions of*  
14 *the Royal Society A: Mathematical, Physical and Engineering Sciences*, 365, 1657-1676,  
15 doi:10.1098/rsta.2007.2036, 2007b.

16 Weintraub, M. N., and Schimel, J. P.: Nitrogen cycling and the spread of shrubs control  
17 changes in the carbon balance of Arctic tundra ecosystems, *BioScience*, 55, 408-415,  
18 doi:10.1641/0006-3568(2005)055[0408:ncatso]2.0.co;2, 2005.

19 Zanina, O. G., Gubin, S. V., Kuzmina, S. A., Maximovich, S. V., and Lopatina, D. A.: Late-  
20 Pleistocene (MIS 3-2) palaeoenvironments as recorded by sediments, palaeosols, and ground-  
21 squirrel nests at Duvanny Yar, Kolyma Lowland, northeast Siberia, *Quaternary Science*  
22 *Reviews*, 30, 2107–2123, doi:10.1016/j.quascirev.2011.01.021, 2011.

23

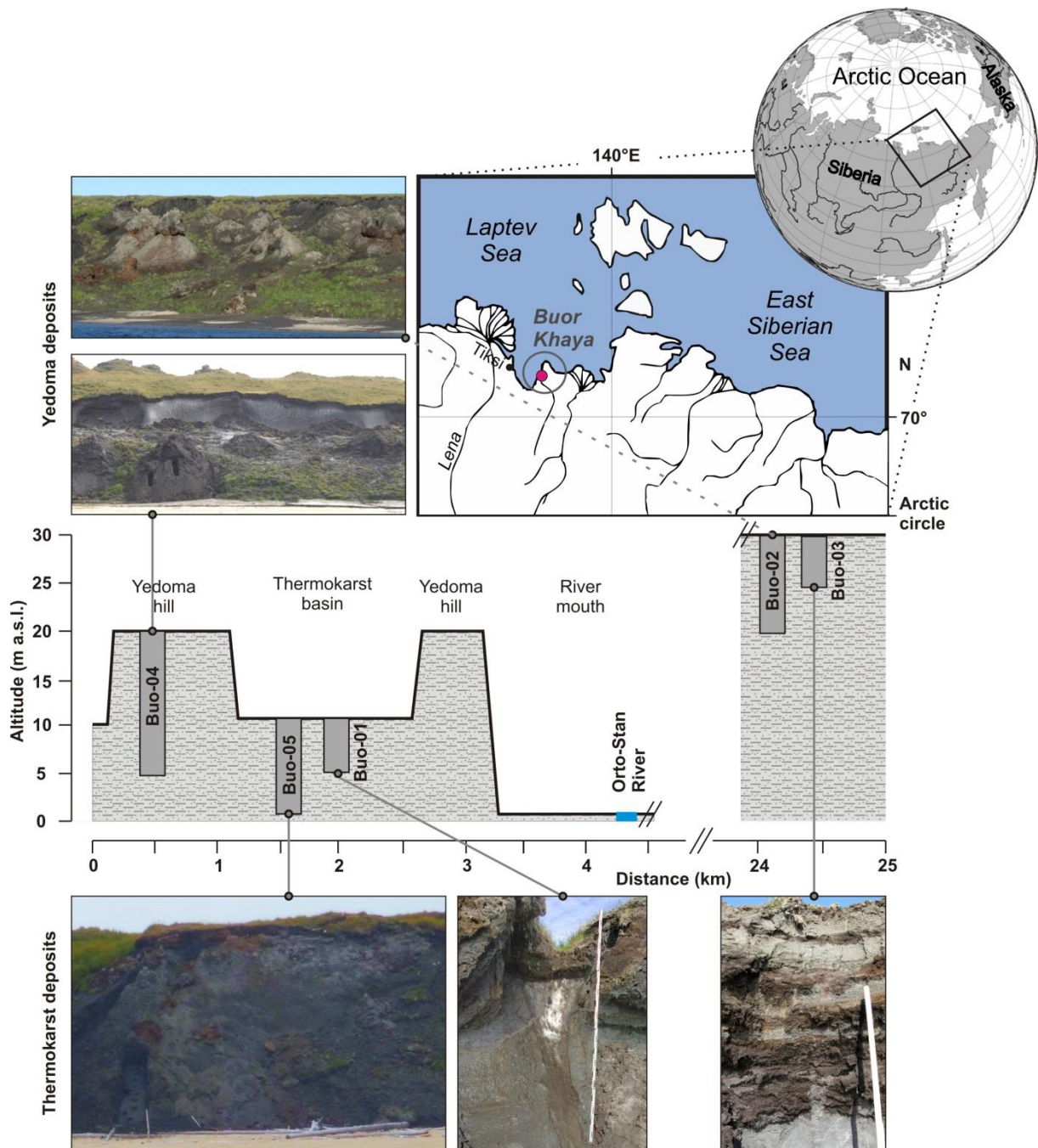
1 Table 1: Radiocarbon AMS dating on plant macro remains. Calibrations were done by using  
 2 Calib 6.0 software and the IntCal09 calibration curve (Stuiver et al., 2010). Depth is given in  
 3 meter below surface level (m b.s.l.) and height in meter above sea level (m a.s.l.). Age is  
 4 given as year before present (a BP). Poz: Poznań Radiocarbon Laboratory, Poland.

Lab. no.	Sample name	Depth [m b.s.l.]	Height [m a.s.l.]	Radiocarbon ages [a BP]	±	Calibrated ages 2σ 95.4% [a BP]	±
Poz-42080	Buo-03-A-03	1.3	28.7	4760	40	5519	70
Poz-42072	Buo-01-A-02	0.7	8.7	3665	35	3990	100
Poz-42073	Buo-01-A-04	1.8	7.6	8140	50	9075	78
Poz-42086	Buo-05-A-04	0.8	8.7	5990	40	6837	103
Poz-42087	Buo-05-B-10	3.4	6.1	8000	80	8817	215
Poz-42088	Buo-05-B-19	6.1	3.4	7940	50	8811	122
Poz-42090	Buo-05-C-23	7.3	2.2	5280	35	6059	74
Poz-42091	Buo-05-C-29	9.2	0.3	6710	90	7566	138
Poz-42074	Buo-02-A-03	0.7	29.3	30,100	300	34613	596
Poz-42075	Buo-02-B-09	3.5	26.5	34,650	550	39813	1242
Poz-42076	Buo-02-B-12	5	25	41,500	1500	45312	2649
Poz-42077	Buo-02-D-20	5.5	24.5	45,000	2000	47614	2386
Poz-42078	Buo-02-D-23	7	23	43,000	1500	46,830	2678
Poz-42081	Buo-04-A-02	1.5	17.1	49,000	3000		
Poz-42082	Buo-04-A-08	5	13.6	>48,000			
Poz-42083	Buo-04-B-10	8.5	9.1	>55,000			
Poz-42084	Buo-04-C-16	10.5	8	>49,000			
Poz-42085	Buo-04-C-20	11.7	6.8	>55,000			

thermocarst deposits

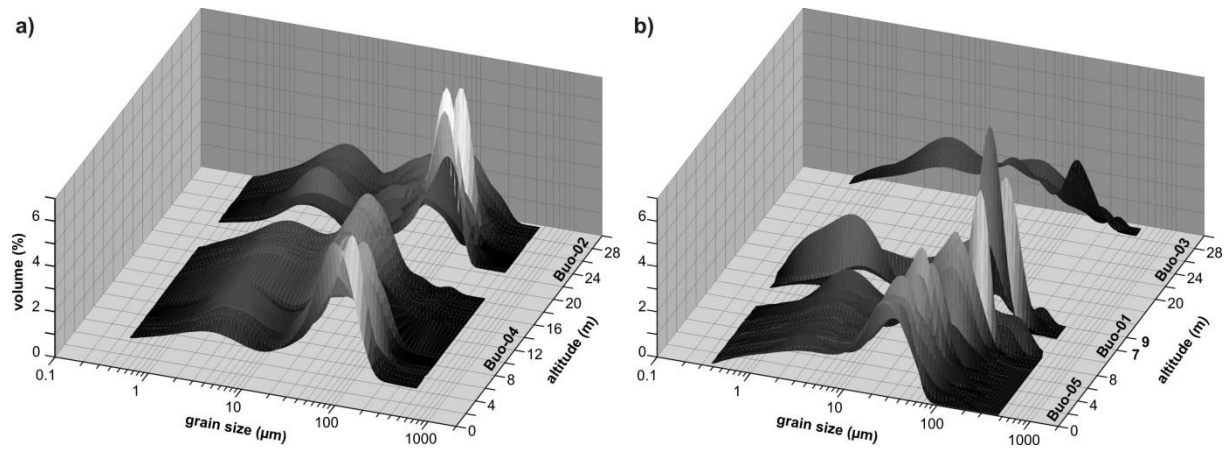
Yedoma deposits

5



1  
2  
3  
4  
5  
6

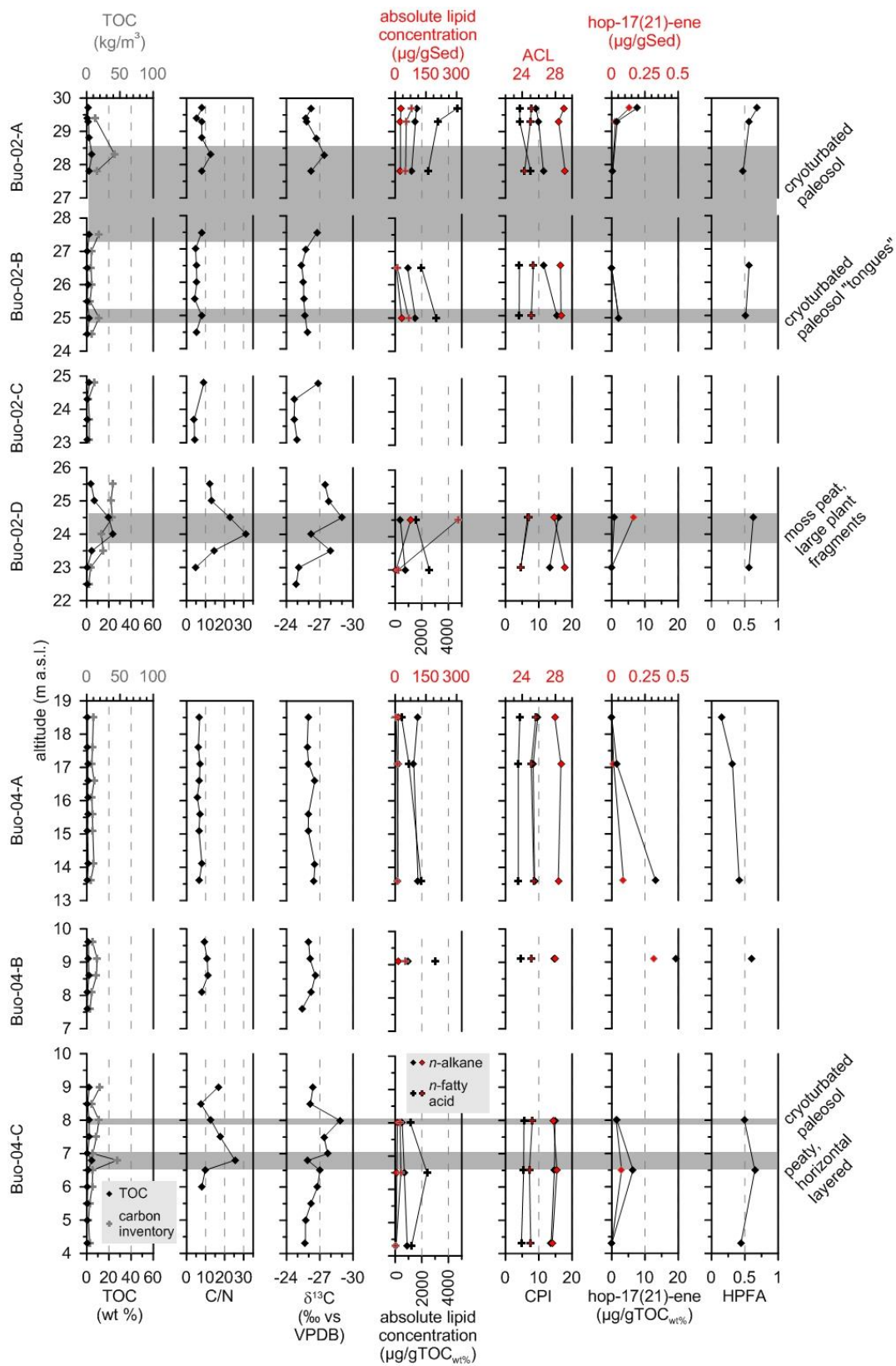
Figure 1. Location of the Buor Khaya Peninsula and the study area. The square black box in the globe inset indicates the area shown in the map below. The profile diagram and the photographs below it show the profiles and their positions relative to each other. Modified after Strauss and Schirmer (2011), pictures taken by J. Strauss.



1

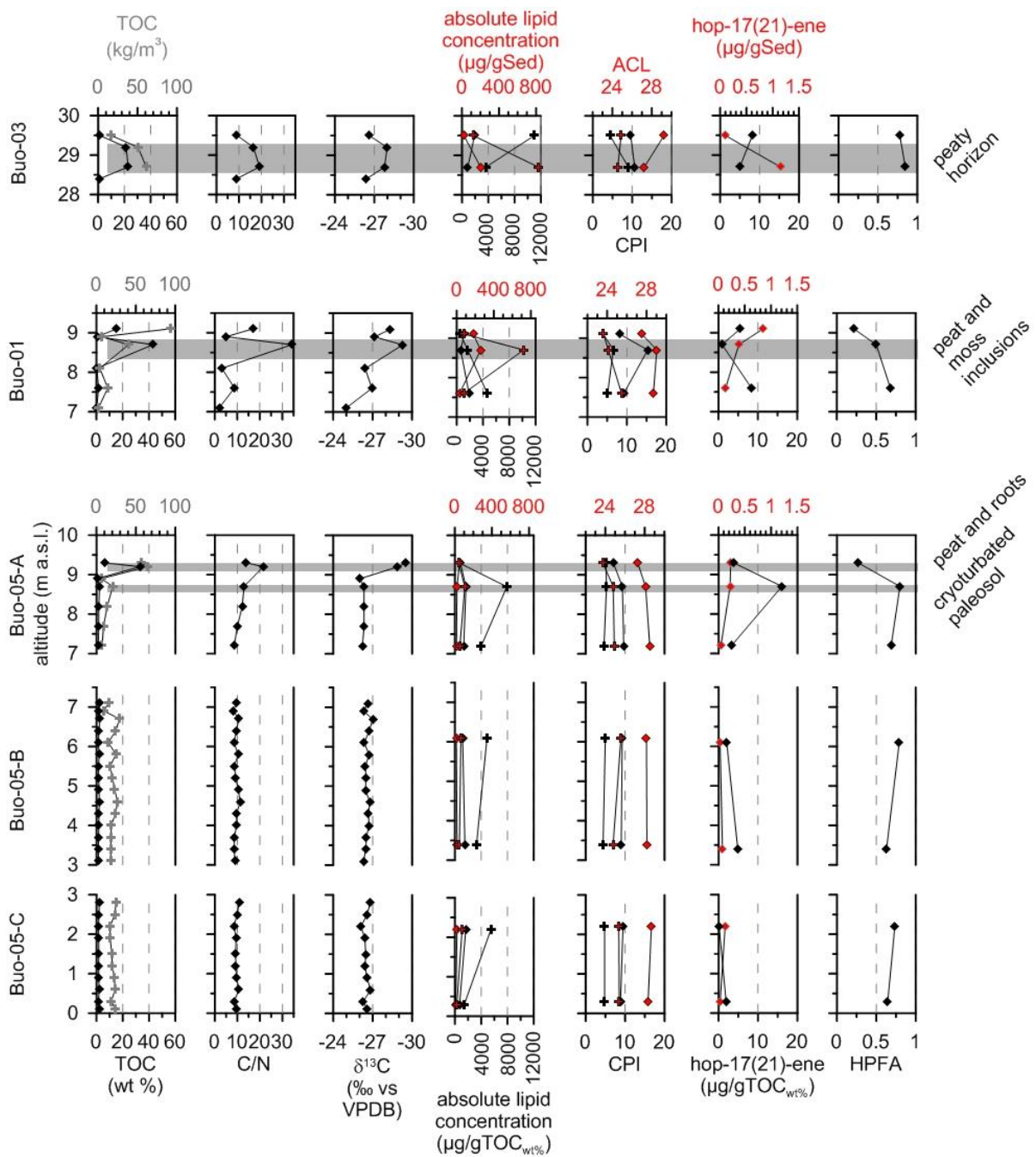
2 Figure 2. Three-dimensional grain-size distributions of a) Yedoma and b) thermokarst  
 3 profiles. To avoid an overlap of Buoy-05 and Buoy-01 in b), the altitude axis was adapted and  
 4 does not ascend consistently. A two-dimensional grain-size plot is shown in Fig. S1.

5



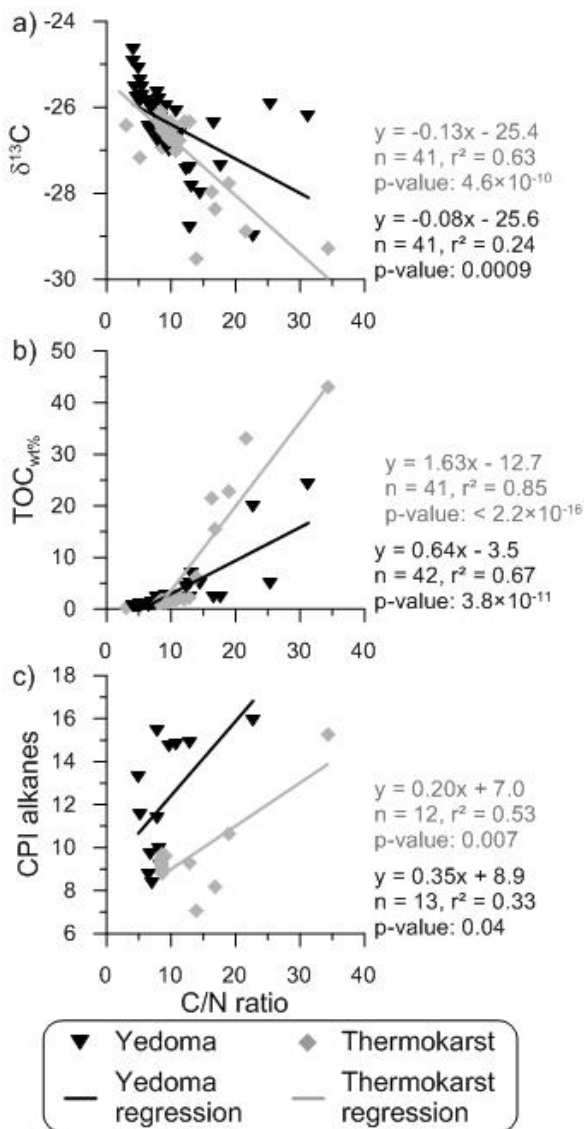
1  
 2 Figure 3. Summary of sedimentological, biogeochemical, and biomarker parameters for the  
 3 Buo-04 and Buo-02 Yedoma profiles. All diagrams are drawn in such a way as to show more  
 4 degraded samples on the left and less degraded samples on the right side. Thus, the axis of

1  $\delta^{13}\text{C}$  values is descending. In the text, the paleocryosol parts are reported with altitude  
 2 measurements from the lowest to the highest sample of each paleocryosol. The grey shaded  
 3 areas are for visualization, not for exact height estimations of the paleocryosols.

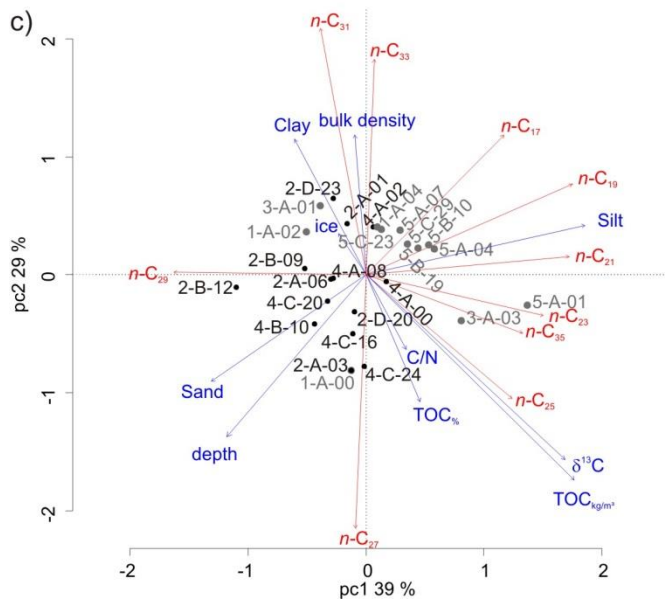
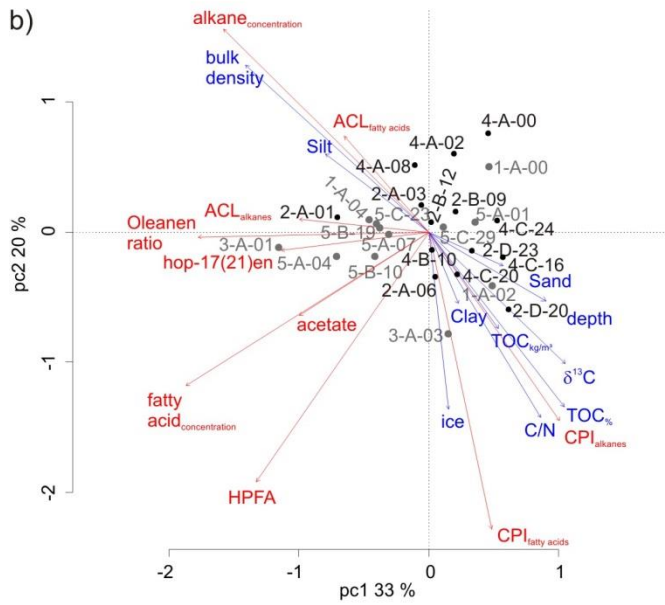
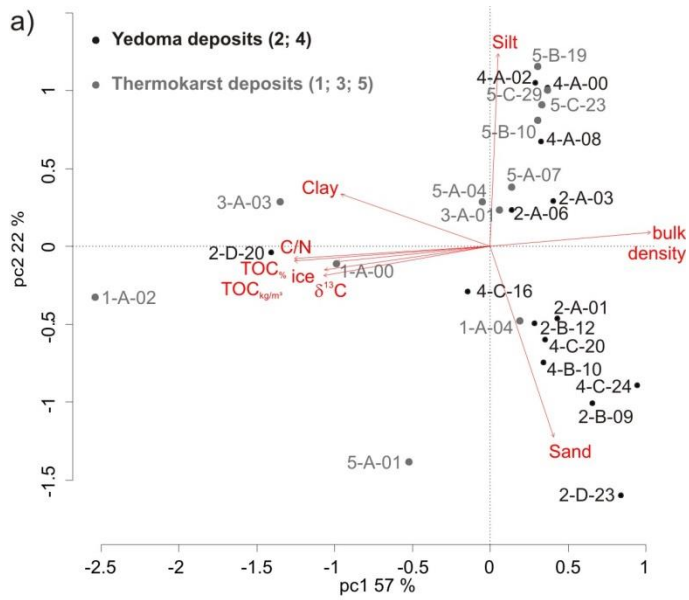


4  
 5 Figure 4. Summary of sedimentological, biogeochemical, and biomarker parameters for the  
 6 Buo-05, Buo-01, and Buo-03 thermokarst profiles. The *n*-alkane and *n*-fatty acid symbols are  
 7 explained in Fig. 3. All diagrams are drawn in such a way as to show more degraded samples  
 8 on the left and less degraded samples on the right side (descending axis of  $\delta^{13}\text{C}$  values). In the  
 9 text, the paleocryosol parts are reported with altitude measurements from the lowest to the

1 highest sample of each paleocrysol. The grey shaded areas are for visualization, not for exact  
 2 height estimations of the paleocrysol.  
 3



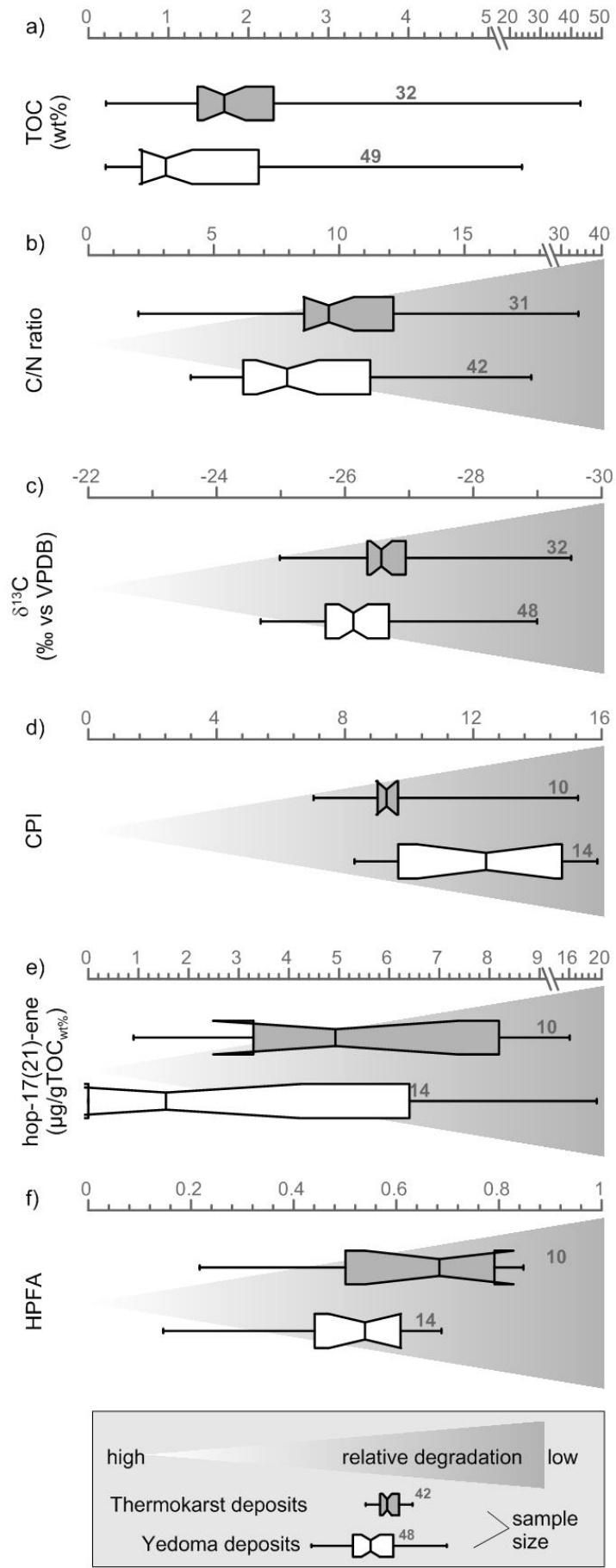
4  
 5 Figure 5. Scatter plots of selected degradation markers. The x-axis shows the C/N ratio  
 6 always. Yedoma deposits are shown as black triangles, thermokarst deposits as grey  
 7 diamonds. Regression equations, the  $r^2$ , sample number (n) and the p-value are inserted as  
 8 texts.  
 9





1 Figure 6. Ordination plots of the principal component analyses (PCA). In diagram a) the  
2 sedimentological parameters are plotted. In b) a PCA of biomarker proxies is shown.  
3 Supplementary variables (in blue: TOC<sub>wt%</sub>, C/N,  $\delta^{13}\text{C}$ , grain size, BD, ice content) were added  
4 without including them in the PCA calculation. In diagram c) the PCA of the major odd *n*-  
5 alkanes is visualized using the same supplementary variables as in b).

6



1 Figure 7. Conceptual scheme of the organic matter degradation state, estimated using the  
2 different applied proxies with boxplots. The merged profiles of Yedoma deposit boxplots  
3 (white boxes) are shown below the thermokarst deposits (grey boxes). The whiskers illustrate  
4 the data range, and the box ends indicate the 25<sup>th</sup> and the 75<sup>th</sup> quartile (interquartile range).  
5 The vertical lines inside each box show the median (=50<sup>th</sup> quartile) including the 95%  
6 confidence intervals, illustrated as notches. All diagrams are drawn in such a way as to show  
7 more degraded samples on the left and less degraded samples on the right side. Thus, the axis  
8 of  $\delta^{13}\text{C}$  values is descending.